

HYPERBOLIC STRUCTURES ON LINK COMPLEMENTS, OCTAHEDRAL DECOMPOSITIONS, AND QUANTUM \mathfrak{sl}_2

Calvin McPhail-Snyder
DUKE UNIVERSITY
UNC CHAPEL HILL

ABSTRACT

Hyperbolic structures (equivalently, principal $\mathrm{PSL}_2(\mathbb{C})$ -bundles with connection) on link complements can be described algebraically by using the *octahedral decomposition*, which assigns an ideal triangulation to any diagram of the link. The decomposition (like any ideal triangulation) gives a set of *gluing equations* in *shape parameters* whose solutions are hyperbolic structures. We show that these equations are closely related to a certain presentation of the *Kac-de Concini quantum group* $\mathcal{U}_q(\mathfrak{sl}_2)$ in terms of cluster algebras at $q = \xi$ a root of unity. Specifically, we identify ratios of the shape parameters of the octahedral decomposition with central characters of $\mathcal{U}_\xi(\mathfrak{sl}_2)$. The quantum braiding on these characters is known to be closely related to $\mathrm{SL}_2(\mathbb{C})$ -bundles on link complements, and our work provides a geometric perspective on this construction.

CONTACT:

Email: calvin@esselltwo.com

Web: www.esselltwo.com

CONTENTS

1	Introduction	1
1.1	Plan of the paper	2
1.2	Hyperbolic 3-manifolds and $\mathrm{SL}_2(\mathbb{C})$ -structures	2
1.3	Ideal triangulations	3
1.4	Quantum holonomy invariants	4
2	The shape biquandle	5
2.1	Shaped link diagrams	5
2.2	The holonomy of a shaped diagram	9
2.3	Biquandle factorizations and the existence of shapings	10
3	The octahedral decomposition and hyperbolic geometry	12
3.1	Ideal octahedra and their shapes	12
3.2	Conventions on ideal tetrahedra	15
3.3	The four-term decomposition	16
3.4	The five-term decomposition	21
4	Decorated representations	23
4.1	Peripheral subgroups and decorations	23
4.2	The meridians	26
4.3	The longitudes	28
5	A connection to quantum groups	30
5.1	Quantum groups at roots of unity	30
5.2	The braiding at a root of unity	32
5.3	Cluster algebras and the Weyl presentation	34
6	Gluing equations	36
6.1	The b -shape variety \mathfrak{B}_D and the segment equations	37
6.2	The a -shape variety \mathfrak{A}_D and the region equations	38
6.3	The segment equations of a twist region	40

1. INTRODUCTION

Let L be a link in S^3 . In low-dimensional topology, it is frequently useful to understand representations $\rho : \pi_1(S^3 \setminus L) \rightarrow \mathrm{SL}_2(\mathbb{C})$, or in our language $\mathrm{SL}_2(\mathbb{C})$ -structures. A major motivation is hyperbolic geometry, because the isometry group $\mathrm{Isom}(\mathbb{H}^3) = \mathrm{PSL}_2(\mathbb{C})$ of hyperbolic 3-space is double-covered by $\mathrm{SL}_2(\mathbb{C})$. In particular, the complete finite-volume hyperbolic metric on a hyperbolic knot corresponds to a distinguished $\rho : \pi_1(S^3 \setminus L) \rightarrow \mathrm{SL}_2(\mathbb{C})$, so computing hyperbolic structures is a special case of our problem.

In this article, we discuss algebraic methods for computing $\mathrm{SL}_2(\mathbb{C})$ -structures on link complements. A *shape* is an ordered triple $\chi = (a, b, m) \in (\mathbb{C} \setminus \{0\})^3$ of nonzero complex numbers. A link diagram is *shaped* when each segment is colored with a shape and the shapes satisfy certain algebraic relations at the crossings. We show that:

1. A shaping of a diagram D of a link L corresponds to an $\mathrm{SL}_2(\mathbb{C})$ -structure (a representation $\rho : \pi_1(S^3 \setminus L) \rightarrow \mathrm{SL}_2(\mathbb{C})$) and up to conjugacy every $\mathrm{SL}_2(\mathbb{C})$ -structure arises in this way.
2. The shapes of a diagram correspond in a simple and explicit way to the shape parameters of the ideal tetrahedra of the octahedral decomposition associated to the diagram.

3. The relations between the shapes at a crossing are determined by the braiding on the quantum group $\mathcal{U}_\xi(\mathfrak{sl}_2)$ for ξ a root of unity.

Previously Blanchet et al. [Bla+20] have shown versions of 1 and 3, and Kim, Kim, and Yoon [KKY18] have shown versions of 1 and 2. Closely related to their work is a description of boundary-parabolic $\mathrm{SL}_2(\mathbb{C})$ -structures for braid closures in terms of cluster variables due to Hikami and Inoue [HI15].

This paper improves these results and places them in a unified context. Our key idea is to consider a presentation of $\mathcal{U}_\xi(\mathfrak{sl}_2)$ in terms of a quantum cluster algebra. This presentation leads to cluster-type coordinates on the $\mathrm{SL}_2(\mathbb{C})$ -representation variety of a tangle complement, which are in turn naturally related to the octahedral decomposition.

1.1. Plan of the paper

- In the remainder of the introduction we give more background on the hyperbolic geometry of 3-manifolds and connections to quantum topology.
- In Section 2 we define shaped tangle diagrams and explain how they relate to $\mathrm{SL}_2(\mathbb{C})$ -structures. We give an algebraic proof that, for any diagram D of a link L , up to conjugacy every $\mathrm{SL}_2(\mathbb{C})$ -structure on L is detected by a shaping of D . We also give some examples of shaped link diagrams.
- In Section 3 we relate shaped tangle diagrams to geometry using the octahedral decomposition. We use this perspective to strengthen our existence result: we can always find geometrically nondegenerate shapings for any nontrivial $\mathrm{SL}_2(\mathbb{C})$ -structure.
- In Section 4 we show how to compute the eigenvalues of the restriction of ρ to the peripheral subgroups of $\pi_1(S^3 \setminus L)$. This is closely related to a *decoration* of the representation.
- In Section 5 we explain the connection to quantum groups and cluster algebras. This perspective allows us to interpret our results as a stronger version of the Hikami-Inoue conjecture [HI15] and its solution by Cho, Yoon, and Zickert [CYZ20].
- In Section 6 we explain how to compute $\mathrm{SL}_2(\mathbb{C})$ -structures in practice: if we restrict to geometrically non-degenerate structures, then we can eliminate half the variables. As an example, we compute all shapings of $(2, 2n + 1)$ -torus knots corresponding to irreducible holonomy representations.

1.2. Hyperbolic 3-manifolds and $\mathrm{SL}_2(\mathbb{C})$ -structures

A manifold is *hyperbolic* if it admits a complete, finite-volume Riemannian metric of curvature -1 . Following Thurston [Thu02], it is more helpful to describe the hyperbolic structure on a 3-manifold M as a $(\mathrm{Isom}(\mathbb{H}^3), \mathbb{H}^3)$ structure. Informally, this means that instead of just building M out of open sets glued together with continuous maps, we build it out of subsets of hyperbolic 3-space \mathbb{H}^3 glued together with hyperbolic isometries. We can further abstract these gluing maps into a representation

$$\rho : \pi_1(M) \rightarrow \mathrm{Isom}(\mathbb{H}^3) = \mathrm{PSL}_2(\mathbb{C})$$

called the *holonomy* of the hyperbolic structure. It is well-defined up to conjugation, and this gives us an algebraic way to study hyperbolic structures. We consider a slightly more general idea:

[Bla+20] C. Blanchet et al., “Holonomy braidings, biquandles and quantum invariants of links with $\mathrm{SL}_2(\mathbb{C})$ flat connections”. [arXiv](#) [DOI](#)

[KKY18] H. Kim, S. Kim, and S. Yoon, “Octahedral developing of knot complement. I: Pseudo-hyperbolic structure”. [arXiv](#) [DOI](#)

[HI15] K. Hikami and R. Inoue, “Braids, complex volume and cluster algebras”. [arXiv](#) [DOI](#)

[CYZ20] J. Cho, S. Yoon, and C. K. Zickert, “On the Hikami-Inoue conjecture”. [arXiv](#) [DOI](#)

[Thu02] W. Thurston, *The geometry and topology of three-manifolds*

DEFINITION 1.1. An $\mathrm{SL}_2(\mathbb{C})$ -*structure* on a 3-manifold M is a representation

$$\rho : \pi_1(M) \rightarrow \mathrm{SL}_2(\mathbb{C}).$$

We call the pair (M, ρ) a $\mathrm{SL}_2(\mathbb{C})$ -*manifold*. Two $\mathrm{SL}_2(\mathbb{C})$ -structures ρ, ρ' are *conjugate* or *gauge-equivalent* if $\rho' = g\rho g^{-1}$ for some $g \in \mathrm{SL}_2(\mathbb{C})$.¹ A $\mathrm{SL}_2(\mathbb{C})$ -structure is *hyperbolic* (gives a complete finite-volume metric) when ρ is discrete and faithful.

To study the hyperbolic geometry of M it suffices to find only the hyperbolic ρ . Remarkably, such a ρ is unique (up to conjugacy and multiplication by ± 1) and when it exists is determined by $\pi_1(M)$; this fact is known as Mostow-Prasad rigidity. However, for a few reasons we are interested instead in computing *all* $\mathrm{SL}_2(\mathbb{C})$ -structures, not just the hyperbolic ones.

MOTIVATING PROBLEM 1. Given a combinatorial description of a 3-manifold M , compute all $\mathrm{SL}_2(\mathbb{C})$ -structures ρ on M .

The space \mathfrak{R}_M of all such ρ is usually called the $\mathrm{SL}_2(\mathbb{C})$ -representation variety of M . Taking the quotient² by the conjugation action of $\mathrm{SL}_2(\mathbb{C})$ gives the $\mathrm{SL}_2(\mathbb{C})$ -character variety \mathfrak{X}_M of M . It determines important information about the topology of M , such as essential surfaces [CS83]. One reason to try to find *all* $\mathrm{SL}_2(\mathbb{C})$ -structures is so that we can understand character varieties.

In this paper we are specifically interested in link complements $M_L := S^3 \setminus L$. From a geometric viewpoint, link complements are slightly different than the closed case: when L has n components M_L is the interior of a compact manifold \overline{M}_L with n torus boundary components. M_L itself is not compact, but we say that it has n *cusps* (corresponding to the boundary components) which we think of as lying at infinity.³ Despite these differences we can still describe the hyperbolic geometry of M_L in terms of $\mathrm{SL}_2(\mathbb{C})$ -structures $\rho : \pi_1(M_L) \rightarrow \mathrm{SL}_2(\mathbb{C})$, which is one reason for introducing them. We can now rephrase our problem as:

MOTIVATING PROBLEM 2. Given a combinatorial description of a link L in S^3 , effectively compute all $\mathrm{SL}_2(\mathbb{C})$ -structures on $M_L = S^3 \setminus L$.

Even if one is only interested in hyperbolic 3-manifolds it is useful to consider more general $\mathrm{SL}_2(\mathbb{C})$ -structures on links, because every hyperbolic 3-manifold M can be obtained as Dehn surgery on an $\mathrm{SL}_2(\mathbb{C})$ -link (L, ρ) . In general, the ρ giving the complete hyperbolic structure on M will give an incomplete structure on the original link complement M_L , so to understand manifolds obtained by surgery we want to compute all of \mathfrak{R}_{M_L} .

1.3. Ideal triangulations

In principle we can compute $\mathrm{SL}_2(\mathbb{C})$ -structures ρ from a presentation $\langle x_i | r_j \rangle$ of $\pi_1(M_L)$: the most obvious method is to introduce a variable for each entry of each matrix $\rho(x_i)$, then consider the algebraic equations in these variables given by the relations r_j . In practice this is usually too difficult unless L is very simple. In addition, these coordinates are not very geometrically enlightening.

Thurston [Thu02] introduced the idea of computing $\mathrm{SL}_2(\mathbb{C})$ -structures using ideal triangulations, which give more tractable equations and a more geometric coordinate system.

DEFINITION 1.2. An *ideal tetrahedron* is a tetrahedron $\Delta \subseteq \mathbb{H}^3$ whose *ideal vertices* lie on the boundary at infinity of \mathbb{H}^3 . An *ideal triangulation* of M_L is a triangulation of M_L by ideal tetrahedra such that the ideal vertices all lie on L .

More formally, let \overline{M}_L be the space obtained by collapsing each component L_j of L to a point P_j . An ideal triangulation of M_L is a triangulation of \overline{M}_L in which the 0-skeleton lies

¹ Sometimes a general representation $\rho : \pi_1(M) \rightarrow \mathrm{PSL}_2(\mathbb{C})$ is called a pseudo-hyperbolic structure. It is convenient for us to also specify a lift to the double cover $\mathrm{SL}_2(\mathbb{C}) \rightarrow \mathrm{PSL}_2(\mathbb{C})$.

² There are some technicalities here: taking a naive quotient by the conjugation action of $\mathrm{SL}_2(\mathbb{C})$ gives a badly-behaved space. Instead the character variety is defined to be $\mathrm{Spec}(\mathfrak{R}_M^{\mathrm{SL}_2(\mathbb{C})})$, where $\mathfrak{R}_M^{\mathrm{SL}_2(\mathbb{C})}$ is the ring of conjugation-invariant functions on the representation variety. Since these issues are not important here, we mostly ignore them.

[CS83] M. Culler and P. B. Shalen, “Varieties of group representations and splittings of 3-manifolds”. DOI

³ A cusped hyperbolic manifold is complete and has finite Riemannian volume, but is non-compact.

entirely on the points $\{P_j\}$.

The geometry of an ideal tetrahedron is described by a *shape parameter* $z \in \mathbb{C} \cup \{\infty\}$. For an ideal triangulation \mathcal{T} of M_L the tetrahedra glue together to give a $\mathrm{SL}_2(\mathbb{C})$ -structure when the shape parameters satisfy *gluing equations*⁴ for each edge of \mathcal{T} . If edges e_i with shape parameters z_i are glued together in \mathcal{T} , then the gluing equation for that edge is

$$\prod_i z_i^{k_i} = 1$$

where z^{k_i} is one of z , $1/(1-z)$, or $1-1/z$ depending on the combinatorics of the triangulation.

We can compute $\mathrm{SL}_2(\mathbb{C})$ -structures⁵ on M_L by specifying an ideal triangulation \mathcal{T} and solving the associated gluing equations. For example, this technique is used by `SNAPPY` [Cul+] to compute hyperbolic structures. However, there are a few drawbacks to this approach:

1. Not all triangulations \mathcal{T} detect all $\mathrm{SL}_2(\mathbb{C})$ -structures: we might need to subdivide \mathcal{T} first.
2. Solving the gluing equations is computationally expensive, and the difficulty grows quickly with the number of tetrahedra.
3. It is not straightforward to recover the matrix coefficients of ρ from the shape parameters; these are needed to compute the quantum holonomy invariants discussed below.
4. Finding an efficient ideal triangulation of a link from its diagram is quite difficult.

The last one is particularly relevant for quantum topology: If we want to work with tangle diagrams and surgery presentations, it is difficult to translate to the language of ideal triangulations and back.

We can address this problem by systematically computing ideal triangulations from link diagrams. The standard way to do this is the *octahedral decomposition*, which was introduced by Thurston [Thu99] and implicit in the work of Kashaev [Kas95, Section 4]. We follow the extensive description by Kim, Kim, and Yoon [KKY18]. The idea is to place an ideal octahedron at each crossing of the link diagram. While the resulting triangulation uses many tetrahedra (4 or 5 per crossing, depending on the version) we can eliminate many of the shape parameters to obtain an efficient description of the gluing equations. In addition, it is possible to reconstruct the map ρ from the shapes of the ideal octahedra.

1.4. Quantum holonomy invariants

One motivation for computing $\mathrm{SL}_2(\mathbb{C})$ -structures on M_L in terms of a diagram of L is to construct *quantum holonomy invariants*. These are enhanced versions of ordinary quantum invariants (like the Jones polynomial) that depend on a choice of $\mathrm{SL}_2(\mathbb{C})$ -structure. A representative example is a construction of Blanchet et al. [Bla+20, Corollary 6.11], as extended in the author's thesis [McP21]:

THEOREM 1.3. Let L be an oriented link in S^3 with components L_1, \dots, L_n , and let ρ be an $\mathrm{SL}_2(\mathbb{C})$ -structure on M_L . Then for each integer $N \geq 2$ there is an invariant

$$F_N(L, \rho, \mathfrak{s}) \in \mathbb{C}$$

defined up to multiplication by $2N$ th roots of unity. It depends only on the isotopy class of L and the conjugacy class of ρ . Furthermore, when $\rho = 1$ is the trivial representation,

$$F_N(L, 1, \mathfrak{s}) = J_N(L)$$

⁴ Usually we also consider some extra equations that ensure the restriction of ρ the boundary tori of M_L has the right eigenvalues; we will discuss these later.

⁵ More accurately, the shape parameters compute $\mathrm{PSL}_2(\mathbb{C})$ -structures.

[Cul+] M. Culler et al., *Snappy, a computer program for studying the geometry and topology of 3-manifolds*

[Thu99] D. Thurston, *Hyperbolic volume and the Jones polynomial*

[Kas95] R. Kashaev, "A link invariant from quantum dilogarithm". [arXiv](#) [DOI](#)

[McP21] C. McPhail-Snyder, "SL₂(C)-holonomy invariants of links". [arXiv](#)

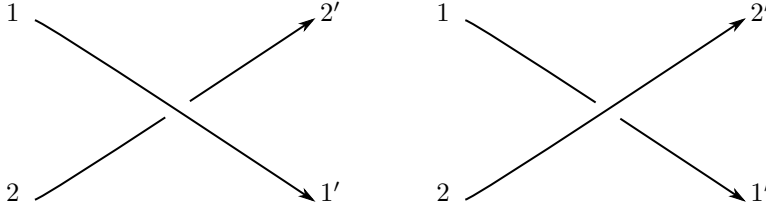


Figure 2: Positive (left) and negative (right) crossings.

is (up to an overall normalization) the colored Jones polynomial of L evaluated at $q = \exp(\pi i/N)$, also known as the Kashaev invariant [MM01]. \diamond

REMARK 1.4. Here \mathfrak{s} is a type of generalized spin structure on M_L . Specifically, if x_i is a meridian of the i th component of L , then \mathfrak{s} is a choice of complex numbers μ_i such that μ_i^N is an eigenvalue of $\rho(x_i)$ for each i . In addition, there are some restrictions when $\text{tr } \rho(x_i) = \pm 2$ [McP21, Introduction §3].

Computing holonomy invariants like F_N requires efficiently computing $\text{SL}_2(\mathbb{C})$ -structures on links in a particular coordinate system related to the quantum group $\mathcal{U}_q(\mathfrak{sl}_2)$. In the language of [Bla+20], we must use the *factorized biquandle* associated to $\text{SL}_2(\mathbb{C})^*$ instead of the *conjugation quandle* of $\text{SL}_2(\mathbb{C})$. Remarkably, this coordinate system is naturally connected to the octahedral decomposition, and describing this connection is a major motivation for this paper.

Acknowledgements

I would like to thank Ian Agol for several helpful conversations about hyperbolic knot theory and Seokbeom Yoon for informing me about the recurrences in Remark 6.18.

This paper is an elaboration of ideas first published in my thesis [McP21]. The presentation of $\mathcal{U}_q(\mathfrak{sl}_2)$ leading to the shape coordinates on tangles was originally discovered by Nicolai Reshetikhin; future joint work [MR22] will apply the ideas in this paper to quantum holonomy invariants.

2. THE SHAPE BIQUANDLE

2.1. Shaped link diagrams

DEFINITION 2.1. Let L be a link in S^3 with n components with a link diagram D . We assume all link diagrams are oriented. Thinking of D as a decorated 4-valent graph G embedded in S^2 , the *segments* of D are the edges⁶ of G . A *region* of a diagram is a connected component of the complement of G , equivalently a vertex of the dual graph of G .

For example, Figure 1 shows an (oriented) diagram with the segments labeled. In an oriented diagram all crossings are positive or negative, as shown in Figure 2. Our preference is to read crossings left-to-right. As shown there, we usually refer to the segments at a given crossing by 1, 2, 1', and 2'. We similarly refer to the regions touching the crossing as N , S , E , and W . The labeling conventions are summarized in Figure 3.

DEFINITION 2.2. A *shape* is a triple of nonzero complex numbers. We usually denote a shape by $\chi = (a, b, m) \in (\mathbb{C} \setminus \{0\})^3$, and when it is assigned to a segment i of a tangle diagram we denote it $\chi_i = (a_i, b_i, m_i)$.

[MM01] H. Murakami and J. Murakami, “The colored Jones polynomials and the simplicial volume of a knot”. [arXiv](#) [DOI](#)

[MR22] C. McPhail-Snyder and N. Reshetikhin, “The R -matrix for cyclic quantum \mathfrak{sl}_2 -modules”

⁶ Usually these are called the “edges” of the diagram, but we do not want to confuse them with edges of ideal polyhedra.

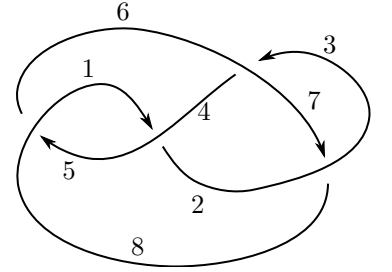


Figure 1: A diagram of the figure-eight knot, with the 8 segments indexed by 1, ..., 8.

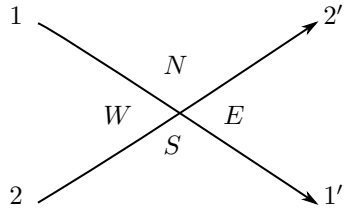


Figure 3: Segments and regions near a crossing.

REMARK 2.3. We can think of a shape as:

- An element of the group $\mathrm{SL}_2(\mathbb{C})^*$:

$$(a, b, m) = \left(\begin{bmatrix} a & 0 \\ (a - 1/m)/b & 1 \end{bmatrix}, \begin{bmatrix} 1 & (a - m)b \\ 0 & a \end{bmatrix} \right) \\ \in \left\{ \left(\begin{bmatrix} \kappa & 0 \\ \phi & 1 \end{bmatrix}, \begin{bmatrix} 1 & \epsilon \\ 0 & \kappa \end{bmatrix} \right) \mid \kappa \neq 0 \right\} = \mathrm{SL}_2(\mathbb{C})^* \subseteq \mathrm{GL}_2(\mathbb{C}) \times \mathrm{GL}_2(\mathbb{C})$$

Here $\mathrm{SL}_2(\mathbb{C})^*$ is the *Poisson dual group* [McP21, Section 0.1] of $\mathrm{SL}_2(\mathbb{C})$.

- A central character of $\mathcal{U}_\xi(\mathfrak{sl}_2)$ for ξ a root of unity.
- Data determining the shapes (complex dihedral angles) of the octahedral decomposition of a link diagram. In the language of Kim, Kim, and Yoon [KKY18] the b_i and m_i correspond to segment variables and a_i and m_i to (ratios of) region variables.
- Data determining the value of an $\mathrm{SL}_2(\mathbb{C})$ -structure ρ on the meridian around a segment of a knot diagram.

DEFINITION 2.4. The *braiding* B is the partially-defined map given by $B(\chi_1, \chi_2) = (\chi_{2'}, \chi_{1'})$, where

$$\begin{aligned} a_{1'} &= a_1 A^{-1} \\ a_{2'} &= a_2 A \end{aligned} \tag{1}$$

$$\begin{aligned} A &= 1 - \frac{m_1 b_1}{b_2} \left(1 - \frac{a_1}{m_1} \right) \left(1 - \frac{1}{m_2 a_2} \right) \\ b_{1'} &= \frac{m_2 b_2}{m_1} \left(1 - m_2 a_2 \left(1 - \frac{b_2}{m_1 b_1} \right) \right)^{-1} \end{aligned} \tag{2}$$

$$\begin{aligned} b_{2'} &= b_1 \left(1 - \frac{m_1}{a_1} \left(1 - \frac{b_2}{m_1 b_1} \right) \right) \\ m_{1'} &= m_1 \quad m_{2'} = m_2 \end{aligned} \tag{3}$$

We think of B as being associated to a positive crossing with incoming strands 1 and 2 and outgoing strands $2'$ and $1'$, as in Figure 3.

B is a partially-defined map on the space of pairs of shapes, and it satisfies braid relations; in Section 2.3 will formalize this by saying that B gives a *generically defined biquandle* [Bla+20, Section 5].

LEMMA 2.5. The map B is generically invertible, and if $(\chi_{2'}, \chi_{1'}) = B^{-1}(\chi_1, \chi_2)$, then

$$\begin{aligned} a_{1'} &= a_1 \tilde{A}^{-1} \\ a_{2'} &= a_2 \tilde{A} \end{aligned} \tag{4}$$

$$\begin{aligned} \tilde{A} &= 1 - \frac{b_2}{m_1 b_1} (1 - m_1 a_1) \left(1 - \frac{m_2}{a_2} \right). \\ b_{1'} &= \frac{m_2 b_2}{m_1} \left(1 - \frac{a_2}{m_2} \left(1 - \frac{m_1 b_1}{b_2} \right) \right) \end{aligned} \tag{5}$$

$$\begin{aligned} b_{2'} &= b_1 \left(1 - \frac{1}{m_1 a_1} \left(1 - \frac{m_1 b_1}{b_2} \right) \right)^{-1} \\ m_{1'} &= m_1 \quad m_{2'} = m_2 \end{aligned} \tag{6}$$

◇

DEFINITION 2.6. We say that a tangle diagram D is *shaped* if its segments are assigned shapes $\{\chi_i\}$ so that at each positive crossing (labeled as in Figure 3) we have $B(\chi_1, \chi_2) = (\chi_{2'}, \chi_{1'})$, and similarly for negative crossings and B^{-1} . We also require that all of the components of $\chi_{1'}$ and χ_2 lie in \mathbb{C}^\times . For example, this means that at a positive crossing we must assign χ_1 and χ_2 so that

$$A = 1 - \frac{b_2}{m_1 b_1} (1 - m_1 a_1) \left(1 - \frac{m_2}{a_2}\right)$$

is not 0 or ∞ .

EXAMPLE 2.7. Consider the diagram of the trefoil in Figure 4 with the segments labeled by $1, \dots, 6$. An assignment of shapes $\chi_i = (a_i, b_i, m_i)$, $i = 1, \dots, 6$ to the diagram is valid if

$$B(\chi_1, \chi_2) = (\chi_3, \chi_4), B(\chi_3, \chi_4) = (\chi_5, \chi_6), \text{ and } B(\chi_5, \chi_6) = (\chi_1, \chi_2).$$

This immediately implies that $m_1 = m_2 = \dots = m_6 = m$; in general there is only one variable m for each component of the link.⁷ A family of solutions is given by

$$\begin{aligned} \chi_1 &= \left(\frac{b_1 m - b_2}{b_1 - b_3}, b_1, m \right) \\ \chi_2 &= \left(-\frac{b_2^2 m^2 - b_2 b_3 m + b_1 b_3}{(b_1 m - b_2)(b_2 m - b_3)}, b_2, m \right) \\ \chi_3 &= \left(-\frac{b_2 b_3 m^3 + b_1 b_3 m^2 - b_2^2 m^2 - b_1 b_2 m + b_1 b_3}{(b_2 m - b_3)(b_1 - b_3)m}, b_3, m \right) \\ \chi_4 &= \left(\frac{(b_2^2 m^2 - b_2 b_3 m + b_1 b_3)m}{b_2 b_3 m^3 + b_1 b_3 m^2 - b_2^2 m^2 - b_1 b_2 m + b_1 b_3}, \frac{(b_2 m - b_3)b_1}{(b_2 m + b_1 - b_3)m}, m \right) \\ \chi_5 &= \left(-\frac{b_2^2 m^4 - b_2 b_3 m^3 + b_2 b_3 m + b_1 b_3 - b_3^2}{(b_2 m - b_3)(b_1 - b_3)m}, \frac{b_1 b_2 m}{b_2 m + b_1 - b_3}, m \right) \\ \chi_6 &= \left(\frac{(b_2^2 m^2 - b_2 b_3 m + b_1 b_3)m}{b_2^2 m^4 - b_2 b_3 m^3 + b_2 b_3 m + b_1 b_3 - b_3^2}, -\frac{b_1 b_3}{(b_2 m - b_3)m}, m \right) \end{aligned}$$

where b_1, b_2, b_3 can be freely chosen as long as none of the a_i or b_i are 0 or ∞ . It turns out that the choice of b_1, b_2, b_3 does not affect the conjugacy class of the $\text{SL}_2(\mathbb{C})$ -structure determined by this shaping. We show how to compute these solutions in Section 6.3.

In practice, the equations for all the a_i and b_i are usually difficult to solve. We can simplify them by either eliminating the b_i and solving them in terms of the a_i or vice-versa. For example, the solutions in the previous example were determined by first solving for the b_i , then using them to determine the a_i . We discuss this in detail in Section 6. For now, we give two relevant lemmas, which also have a geometric interpretation (see Section 3).

DEFINITION 2.8. A crossing (labeled as in Figure 3) is *pinched* if any of the equations

$$b_2 = m_1 b_1, \quad m_2 b_2 = m_1 b_{1'}, \quad b_{2'} = b_1, \quad m_2 b_{2'} = b_{1'}$$

hold, in which case all of them do. A crossing is *degenerate* if either of the equations

$$a_1 = a_{1'} \text{ or } a_2 = a_{2'}$$

hold, in which case both do. A degenerate crossing is necessarily pinched but a pinched crossing can be non-degenerate.

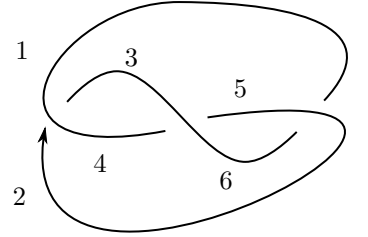


Figure 4: A diagram of the trefoil knot with labeled segments.

⁷ Geometrically, m is an eigenvalue of the holonomy of a meridian, and there is one conjugacy class of meridian per link component.

REMARK 2.9. We will see in Section 3 that a crossing is pinched when the tetrahedra of the four-term decomposition are geometrically degenerate, while it is degenerate if the tetrahedra of the five-term decomposition are geometrically degenerate.

LEMMA 2.10. At a non-pinched positive crossing,

$$\begin{aligned} a_1 &= \frac{b_2 - m_1 b_1}{b_{2'} - b_1} & a_{1'} &= \frac{m_2 b_2 - m_1 b_{1'}}{m_2 b_{2'} - b_{1'}} \\ a_2 &= \frac{b_1}{m_2 b_{1'}} \frac{m_2 b_2 - m_1 b_{1'}}{b_2 - m_1 b_1} & a_{2'} &= \frac{b_1}{m_2 b_{1'}} \frac{m_2 b_{2'} - b_{1'}}{b_{2'} - b_1} \end{aligned} \quad (7)$$

while at a non-pinched negative crossing

$$\begin{aligned} a_1 &= \frac{b_{2'}}{m_1 b_2} \frac{b_2 - m_1 b_1}{b_{2'} - b_1} & a_{1'} &= \frac{b_{2'}}{m_1 b_2} \frac{m_2 b_2 - m_1 b_{1'}}{m_2 b_{2'} - b_{1'}} \\ a_2 &= \frac{m_2 b_2 - m_1 b_{1'}}{b_2 - m_1 b_1} & a_{2'} &= \frac{m_2 b_{2'} - b_{1'}}{b_{2'} - b_1} \end{aligned} \quad (8)$$

◇

Proof. Once we know (7) and (8) it is easy to check them against (1–6). □

LEMMA 2.11. At any non-degenerate positive crossing,

$$\begin{aligned} \frac{b_2}{b_1 m_1} &= \frac{(1 - a_1/m_1)(1 - 1/m_2 a_2)}{1 - a_1/a_{1'}} \\ \frac{m_2 b_{2'}}{b_{1'}} &= \frac{(1 - m_1/a_{1'})(1 - m_2 a_{2'})}{1 - a_1/a_{1'}} \\ \frac{b_1}{b_{2'}} &= \frac{1 - a_{1'}/a_1}{(1 - m_1/a_1)(1 - 1/m_2 a_{2'})} \\ \frac{m_1 b_{1'}}{m_2 b_2} &= \frac{1 - a_{1'}/a_1}{(1 - a_{1'}/m_1)(1 - m_2 a_2)} \end{aligned} \quad (9)$$

while at a non-degenerate negative crossing,

$$\begin{aligned} \frac{b_2}{b_1 m_1} &= \frac{1 - a_1/a_{1'}}{(1 - a_1 m_1)(1 - m_2/a_2)} \\ \frac{m_2 b_{2'}}{b_{1'}} &= \frac{1 - a_1/a_{1'}}{(1 - 1/m_1 a_{1'})(1 - a_{2'}/m_2)} \\ \frac{b_1}{b_{2'}} &= \frac{(1 - 1/m_1 a_1)(1 - m_2/a_{2'})}{1 - a_{1'}/a_1} \\ \frac{m_1 b_{1'}}{m_2 b_2} &= \frac{(1 - m_1 a_{1'})(1 - a_2/m_2)}{1 - a_{1'}/a_1} \end{aligned} \quad (10)$$

◇

Proof. As before, once we know the right equations to check this is a straightforward verification. □

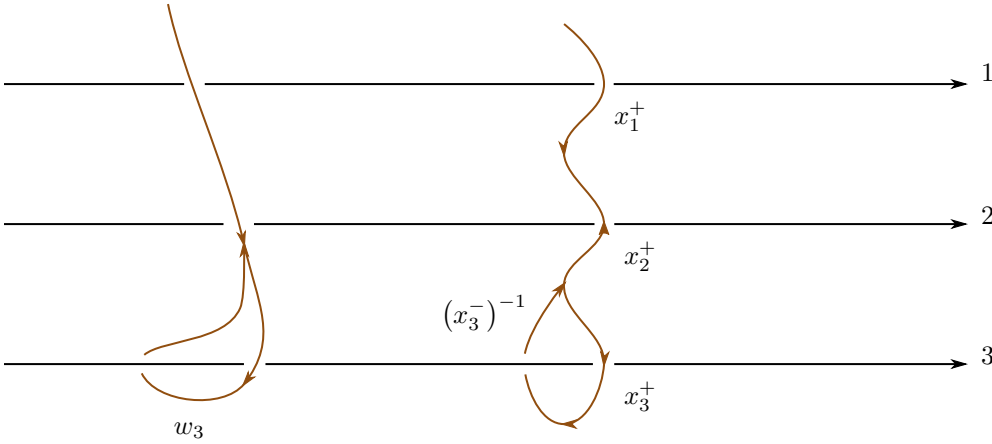


Figure 7: The path w_3 in $\pi_1(M_L)$ and the path $x_1^+ x_2^+ x_3^+ (x_3^-)^{-1} (x_2^+)^{-1} (x_1^+)^{-1}$ in $\Pi_1(D)$ are equivalent.

2.2. The holonomy of a shaped diagram

We can now explain how shaped diagrams relate to $\mathrm{SL}_2(\mathbb{C})$ -structures.

DEFINITION 2.12. Let D be a shaped diagram of L . The *fundamental groupoid* $\Pi_1(D)$ of D has one object for each region of D and two generators x_j^\pm for each segment j . These represent paths above and below the segment, as in Figure 5. There are three relations for each crossing, given by

$$x_1^\pm x_2^\pm = x_2^\pm x_1^\pm \text{ and } \begin{cases} x_1^- x_2^+ = x_2^+ x_1^- & \text{for a positive crossing, or} \\ x_1^+ x_2^- = x_2^- x_1^+ & \text{for a negative crossing.} \end{cases} \quad (11)$$

PROPOSITION 2.13. For any diagram D of a link L , the groupoid $\Pi_1(D)$ is equivalent to the fundamental group $\pi_1(M_L)$ of the link complement. \diamond

To use more abstract language, the claim is that the group $\pi_1(M_L)$ is a skeleton of the groupoid $\Pi_1(D)$.

Proof. A detailed proof is given in [Bla+20, Section 3]. It is instructive to consider an example: In Figure 7, we have expressed a path $w_3 \in \pi_1(M_L)$ representing a generator of the Wirtinger presentation of $\pi_1(M_L)$ in terms of elements of $\Pi_1(D)$. \square

REMARK 2.14. The standard way to study $\pi_1(M_L)$ using a diagram of L is the Wirtinger presentation, which has one generator for each arc (arcs don't break at overcrossings, unlike segments) and one relation for each crossing. We can think of $\Pi_1(D)$ as using a greater number of more local generators. This turns out to be more convenient when we discuss face pairings in Section 3.

DEFINITION 2.15. Let D be a shaped link diagram. The *holonomy representation* of D is the representation

$$\rho : \Pi_1(D) \rightarrow \mathrm{SL}_2(\mathbb{C})$$

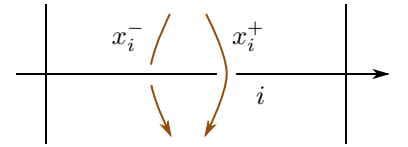


Figure 5: Generators of the fundamental groupoid $\Pi_1(D)$ of a tangle diagram.

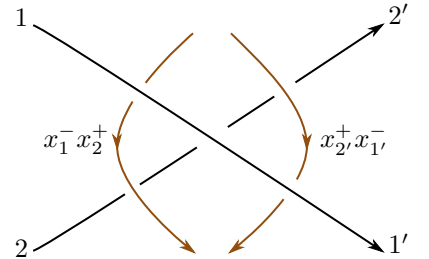


Figure 6: Deriving the middle relation at a crossing.

given by

$$\rho(x^+) = \begin{bmatrix} a & 0 \\ (a - 1/m)/b & 1 \end{bmatrix}, \quad \rho(x^-) = \begin{bmatrix} 1 & (a - m)b \\ 0 & a \end{bmatrix}, \quad (12)$$

where the generators x^\pm are associated to a strand of D colored with the shape $\chi = (a, b, m)$. By Theorem 2.17 below, ρ also gives a representation $\pi_1(M_L) \rightarrow \mathrm{SL}_2(\mathbb{C})$, and we do not usually distinguish between these.

REMARK 2.16. A link group $\pi_1(M_L)$ has certain distinguished elements called meridians, which correspond to paths around a single strand of L . The generators of the Wirtinger presentation are meridians, and all meridians of the same component of L are conjugate. In terms of $\Pi_1(D)$, the meridian around a strand with shape χ is conjugate to the matrix

$$\rho(x^+(x^-)^{-1}) = \begin{bmatrix} a & -(a - m)b \\ (a - 1/m)/b & m + m^{-1} - a \end{bmatrix} \quad (13)$$

which has trace $m + m^{-1}$. In general, the meridian is *not* equal to $\rho(x^+(x^-)^{-1})$, as shown in Figure 7.

THEOREM 2.17. The holonomy representation of $\Pi_1(D)$ is well-defined and gives a representation $\rho : \pi_1(M_L) \rightarrow \mathrm{SL}_2(\mathbb{C})$. \diamond

Proof. To make sure ρ is well-defined, we need to check that the braiding rules on the χ_i are compatible with the relations (11), which is straightforward. Then both claims follow from Proposition 2.13. \square

For this theorem to be useful, we need to make sure that shapings of link diagrams actually give all $\mathrm{SL}_2(\mathbb{C})$ -structures. This is false, but a slightly weaker statement is true. Let L be a link in S^3 and D any oriented diagram of L . In practice we are mostly interested in $\mathrm{SL}_2(\mathbb{C})$ -structures up to conjugation, and we have the following existence theorem:

THEOREM 2.18. We say a decorated $\mathrm{SL}_2(\mathbb{C})$ -structure ρ is *detected* by D if there is a shaping of D with holonomy representation ρ . Every decorated $\mathrm{SL}_2(\mathbb{C})$ -structure on L is conjugate to one detected by D . \diamond

This theorem is one of the major results of Blanchet et al. [Bla+20]. We sketch the proof in the next section. In Theorem 3.10 we give a stronger result: when $\rho \neq \pm 1$ is nontrivial, then up to conjugacy ρ is detected by a *geometrically nondegenerate* shaping.

2.3. Biquandle factorizations and the existence of shapings

Blanchet et al. [Bla+20] have developed a general theory for dealing with coordinate systems like ours by considering two related algebraic structures. We briefly explain how it relates to our example.

DEFINITION 2.19. A *quandle* is a set Q with a binary operation \triangleright such that:

1. For all $a, b, c \in Q$, $a \triangleright (b \triangleright c) = (a \triangleright b) \triangleright (a \triangleright c)$,
2. for all $a, b \in Q$ there is a unique $c \in Q$ such that $a = b \triangleright c$, and
3. for any $a \in Q$, $a \triangleright a = a$.

We say a link diagram is *colored* by a quandle Q if its segments are assigned elements of Q according to the rule in Figure 8 (with a similar one for negative crossings).

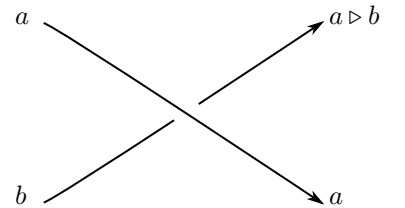


Figure 8: Labeling segments at a crossing using a quandle. Notice that both ends of the over-arc have the same label.

The prototypical example is the conjugation structure of a group:

EXAMPLE 2.20. Let G be a group. The *conjugation quandle* associated to G has $Q = G$ and

$$g \triangleright h = hgh^{-1}.$$

Using the Wirtinger presentation of the fundamental group of a link complement, it is straightforward to see that colorings of diagrams of L by the conjugation quandle of G are exactly the same as representations $\pi_1(M_L) \rightarrow G$. In particular, $\mathrm{SL}_2(\mathbb{C})$ -structures on a link diagram are exactly colorings by the conjugation quandle of $\mathrm{SL}_2(\mathbb{C})$.

However, to construct quantum invariants of links with $\mathrm{SL}_2(\mathbb{C})$ structures a different description is needed. Consider the following factorization of elements⁸ of $\mathrm{SL}_2(\mathbb{C})$:

$$g = \begin{bmatrix} \kappa & -\epsilon \\ \phi & (1 - \epsilon\phi)/\kappa \end{bmatrix} = \begin{bmatrix} \kappa & 0 \\ \phi & 1 \end{bmatrix} \begin{bmatrix} 1 & \epsilon \\ 0 & \kappa \end{bmatrix} = g^+(g^-)^{-1}$$

We can think of the pair (g^+, g^-) as an element of the group

$$\mathrm{SL}_2(\mathbb{C})^* = \left\{ \left(\begin{bmatrix} \kappa & 0 \\ \phi & 1 \end{bmatrix}, \begin{bmatrix} 1 & \epsilon \\ 0 & \kappa \end{bmatrix} \right) \mid \kappa \neq 0 \right\} \subseteq \mathrm{GL}_2(\mathbb{C}) \times \mathrm{GL}_2(\mathbb{C}).$$

Instead of giving the holonomy g around a strand, we split g into the holonomy g^+ from passing above the strand and g^- from passing below. In general this works for any *factorizable algebraic group* [KR05, Section 2]. The motivation for working with group factorizations has to do with the representation theory of quantum groups at roots of unity. If G is a simple Lie group with algebra \mathfrak{g} and ξ is a root of unity, the center of (the Kac-de Concini form of) $\mathcal{U}_\xi(\mathfrak{g})$ is an algebraic group G^* distinct from the Lie group G . In general, G^* is related to G in the same way $\mathrm{SL}_2(\mathbb{C})^*$ is to $\mathrm{SL}_2(\mathbb{C})$. We discuss this in more detail in Section 5.

When passing from G to G^* we pass from the Wirtinger-like relations $g_{1'} = g_1$ and $g_{2'} = g_1 g_2 g_1^{-1}$ to the factorized relations (11). In particular, we have to allow the case $g_{1'}^\pm \neq g_1^\pm$. This is captured by a more general structure called a biquandle.

DEFINITION 2.21. A *biquandle* is a set X together with an invertible map $B = (B_1, B_2) : X \times X \rightarrow X \times X$ such that:

1. The map B satisfies the braid relation:

$$(\mathrm{id} \times B)(B \times \mathrm{id})(\mathrm{id} \times B) = (B \times \mathrm{id})(\mathrm{id} \times B)(B \times \mathrm{id}).$$

2. The map B is sideways invertible: there is a unique bijection $S : X \times X \rightarrow X \times X$ such that

$$S(B_1(x, y), x) = (B_2(x, y), y)$$

for all $x, y \in X$.

3. The map S induces a bijection $\alpha : X \rightarrow X$ on the diagonal:

$$S(x, x) = (\alpha(x), \alpha(x)).$$

We say a link diagram is *colored* by X if its segments are assigned elements of X such that at every positive crossing labeled as in Figure 2,

$$B(x_1, x_2) = (x_{2'}, x_{1'})$$

and similarly for negative crossings and B^{-1} .

⁸ Actually, this only works for a Zariski open subset of $\mathrm{SL}_2(\mathbb{C})$, specifically the matrices with nonzero 1, 1 entry. We will address this shortly by introducing the idea of a generically defined biquandle.

[KR05] R. Kashaev and N. Reshetikhin, “Invariants of tangles with flat connections in their complements”. [arXiv](#) [DOI](#)

A biquandle is a generalization of a quandle, and it is the right language for dealing with factorizations like (13). We think of axiom (2) as saying that specifying any two adjacent elements x_i at a crossing determines the other two, and axiom (3) as regulating the behavior of the biquandle at kinks.

It turns out that in order to handle our coordinate system we need a further generalization than biquandles. The problem is that the map B of Definition 2.4 is only partially defined: there are certain singular pairs (χ_1, χ_2) where, say, $a_{1'}$ becomes 0. The main example [Bla+20, Example 5.2] of a biquandle factorization in the literature is very closely related to our shape coordinates, and suffers from the same problem. To fix it, we can introduce *generically defined biquandles* [Bla+20, Section 5]. The idea is that if such singular pairs are rare (say, the complement of a Zariski open dense set) then we can always avoid them, possibly by global conjugation (also known as gauge transformation).

By using these techniques, proving Theorem 2.18 reduces to showing that the braiding of Definition 2.4 defines a *generic biquandle factorization* of the conjugation quandle of $\mathrm{SL}_2(\mathbb{C})$. The idea is that a biquandle coloring naturally gives a representation of the groupoid $\Pi_1(D)$, while a quandle coloring is more naturally related to $\pi_1(M_L)$, and these need to be compatible as in Theorem 2.17.

Once the general theory is constructed, it is not too hard to show [Bla+20, Theorem 5.5] that a closely related example is a generic factorization of the conjugation quandle of $\mathrm{SL}_2(\mathbb{C})$. We can repeat essentially the same proof to prove Theorem 2.18, with some modifications to one step: In the original proof [Bla+20, Appendix B] we consider the Zariski open subset

$$U = \left\{ \begin{bmatrix} \kappa & -\epsilon \\ \phi & (1 - \epsilon\phi)/\kappa \end{bmatrix} \middle| \kappa, \epsilon, \phi \in \mathbb{C}, \kappa \neq 0 \right\} \subset \mathrm{SL}_2(\mathbb{C})$$

of matrices representable in terms of the factorization $g = g^+(g^-)^{-1}$. In our example, we consider the smaller set

$$U' = \left\{ \begin{bmatrix} a & -(a-m)b \\ (a-1/m)/b & m+m^{-1}-a \end{bmatrix} \middle| a, b, m \in \mathbb{C} \setminus \{0\} \right\} \subset \mathrm{SL}_2(\mathbb{C})$$

which is still Zariski open, so the same argument goes through.

We sketch the argument briefly. Fixing a diagram D we can consider the set of representations $\rho : \pi_1(D) \rightarrow \mathrm{SL}_2(\mathbb{C})$ such that $\rho(x_i) \in U$ for every Wirtinger generator x_i . This is a finite intersection of open sets, so it is again open. By the general theory developed in [Bla+20, Section 5, Appendix A] this is enough to guarantee that every ρ is conjugate to some ρ' with $\rho'(x_i) \in U$ for all i , i.e. to one representable in terms of the factorized matrices g^\pm .

3. THE OCTAHEDRAL DECOMPOSITION AND HYPERBOLIC GEOMETRY

We can now describe a geometric interpretation of our coordinates $\chi_i = (a_i, b_i, m_i)$.

3.1. Ideal octahedra and their shapes

Thurston [Thu02] introduced a way to combinatorially describe hyperbolic structures on link complements (more generally, on cusped 3-manifolds) by using *ideal triangulations*. The idea is to triangulate $S^3 \setminus L$ with all the 0-vertices “at infinity”, that is lying on L ; we can think of this in terms of *ideal polyhedra*, which are polyhedra with their vertices removed.

We can describe hyperbolic structures on ideal polyhedra by splitting them into ideal tetrahedra. The hyperbolic geometry of an ideal tetrahedron is summarized by a *shape parameter*

$z \in \mathbb{C} \setminus \{0, 1\}$ whose argument is the dihedral angle at a particular edge of the tetrahedron. (The shape parameters at the other edges are $1/(1 - z)$ and $1 - 1/z$.) When the ideal simplices are glued together we can check certain *gluing equations* on the parameters at the involved edges; if they are satisfied, we get a hyperbolic structure on the glued manifold. We refer to Purcell [Pur20] for details.

One method to construct ideal triangulations of link complements systematically from diagrams is the *octahedral decomposition* [Thu99; Kas95], which decomposes the link complement into ideal octahedra. We briefly summarize the treatment of Kim, Kim, and Yoon [KKY18]. Fix a diagram D of L . We put an ideal octahedron at each crossing of D with its top and bottom ideal vertices on the strands of the link, labeled as P_1 and P_2 in Figure 9. There are four extra ideal vertices P_+ , P_- , P'_+ , and P'_- , which we pull above and below the diagram, in the process identifying P_+ with P'_+ and P_- with P'_- . The resulting simplicial complex is called a *twisted octahedron*.

The twisted octahedra have two types of edges to glue, which we call *vertical* and *horizontal* edges as in Figure 10. We can determine the gluing patterns of the horizontal edges by looking at the regions of the link diagram D , while the gluing patterns of the vertical edges come from the arcs of D ; see [KKY18, Section 4] for details. The result is an ideal triangulation of $S^3 \setminus (L \cup \{P^+, P_-\})$, where P_\pm are the two extra ideal points above and below the diagram. These extra points are not a problem in practice; because their neighborhoods are balls (not tori) we can cap them off canonically.

Given a *shaped* diagram D of our link L we can assign shape parameters to the edges of the ideal octahedra. The idea is that the a -variables are associated to the vertical edges and the b -variables are associated to the horizontal edges.

DEFINITION 3.1. Let D be a shaped diagram of a link L . Consider a twisted octahedron O at a positive crossing of D . In terms of the characters χ_i of the segments of the crossing, we assign the following shape parameters to the vertical and horizontal edges of O :

$$o_1 = \frac{a_1}{m_1} \quad o_2 = \frac{1}{m_2 a_2} \quad o_{1'} = \frac{m_1}{a_{1'}} \quad o_{2'} = m_2 a_{2'} \quad (14)$$

$$o_N = \frac{b_{2'}}{b_1} \quad o_W = \frac{m_1 b_1}{b_2} \quad o_S = \frac{m_2 b_2}{m_1 b_{1'}} \quad o_E = \frac{b_{1'}}{m_2 b_{2'}} \quad (15)$$

Here by o_j we mean the shape of the vertical edge immediately below or above segment j , and by o_k we mean the shape of the horizontal edge near region k . It may be more convenient to consult Figure 11.

At a negative crossing, we instead assign

$$o_1 = \frac{1}{m_1 a_1} \quad o_2 = \frac{a_2}{m_2} \quad o_{1'} = m_1 a_{1'} \quad o_{2'} = \frac{m_2}{a_{2'}} \quad (16)$$

$$o_N = \frac{b_{2'}}{b_1} \quad o_W = \frac{m_1 b_1}{b_2} \quad o_S = \frac{m_2 b_2}{m_1 b_{1'}} \quad o_E = \frac{b_{1'}}{m_2 b_{2'}} \quad (17)$$

Note that the horizontal shapes (17) are the same as (15).

THEOREM 3.2. For any shaped link diagram D , the shape assignments of Definition 3.1 satisfy the gluing relations of the octahedral decomposition. \diamond

Proof. We refer to [KKY18, Section 3.2] for the derivation of these equations. There are two⁹ types to check: region equations and segment equations. We also need to check the behavior around the cusps (that is, the strands of the link) to make sure it matches the eigenvalues

[Pur20] J. S. Purcell, *Hyperbolic knot theory*. arXiv doi

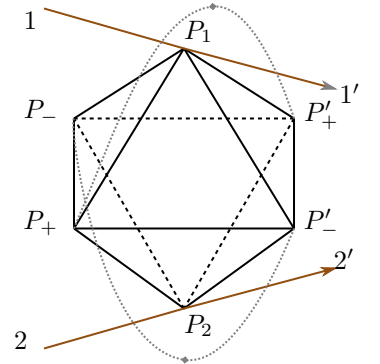


Figure 9: An ideal octahedron at a positive crossing, viewed from the side. The ideal vertices P_+ and P'_+ are identified by pulling them above the diagram, as indicated by the grey curves. The strands of the link are shown in gold.

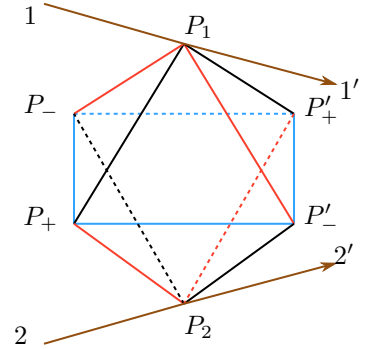


Figure 10: Red *vertical* and blue *horizontal* edges of an octahedron at a positive crossing. (Recall that the edges $P_1 P_+$ and $P_1 P'_+$ are glued in the twisted octahedron, and similarly for $P_2 P_-$ and $P_2 P'_-$.)

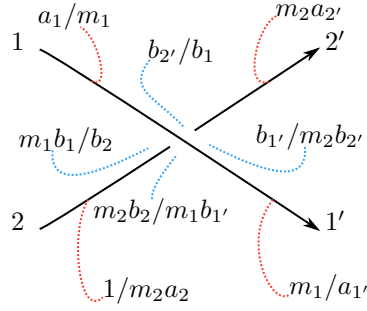


Figure 11: Shapes of edges at a positive crossing. There are four horizontal edges at the four corners and four vertical edges below and above the four segments.

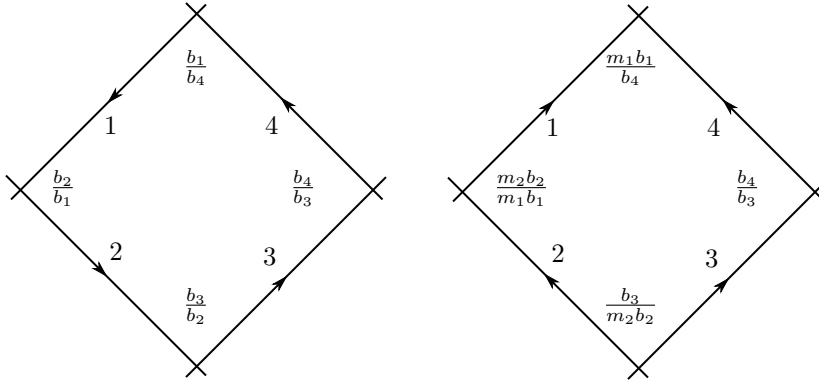


Figure 13: Two examples of the region gluing equations. The product of all the parameters is 1 regardless of the orientation of the boundary segments.

m_j ; doing this carefully requires considering the triangulation of the boundary induced by truncating our tetrahedra.

The region equations [KKY18, eq. 7] say that the product of horizontal edge shapes around any region of the diagram must be 1. It is straightforward to see that this always holds, because the horizontal edge shapes are ratios of parameters assigned to the segments of the diagram, so checking this becomes a combinatorial fact about oriented planar graphs. We give two examples in Figure 13.

The segment equations are more complicated because the vertical edges of the octahedra are glued together along the over-arcs and under-arcs of the diagram. This involves multiple segments at different crossings, so there is something nonlocal to check. A key observation of Kim, Kim, and Yoon is that the vertical edge gluing equations follow from a stronger *local* condition at each segment, which they call the *m-hyperbolicity equations* [KKY18, eq. 10]. We give them in our conventions in Definition 4.9. It is easy to check that the vertical edges at each segment satisfy the corresponding *m-hyperbolicity equation* and this implies that the gluing equations for the vertical edges of all the octahedra hold.

As suggested by the name the *m-hyperbolicity equation* asserts that m really is an eigenvalue of the holonomy of a meridian with shape $\chi = (a, b, m)$; we discuss this further in Section 4. \square

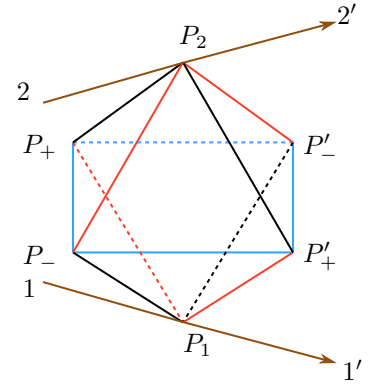


Figure 12: Red **vertical** and blue **horizontal** edges of an octahedron at a negative crossing. Notice that the vertical edges are indexed slightly differently than in the positive case.

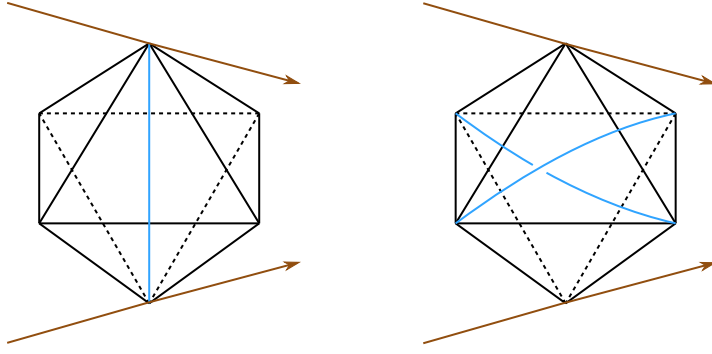


Figure 14: The four-term and five-term decompositions of an octahedron.

We have described the geometry of ideal octahedra, but to connect with the standard language of hyperbolic geometry we need to subdivide these into ideal 3-simplices, that is into ideal tetrahedra. There are two ways (Figure 14) to do this, which we call the *four-term* and *five-term* decompositions. The latter is sometimes more convenient because we can always (see Theorem 3.10) find geometrically nondegenerate shapes for its octahedra, at least when the representation ρ is nontrivial. However, the four-term decomposition is more closely connected to the quantum algebra of Section 5, and in Section 3.3 we use it to prove that the holonomy representation associated to the octahedral decomposition agrees with the algebraically defined holonomy representation of Section 2.

3.2. Conventions on ideal tetrahedra

Before discussing the decomposition of the ideal octahedra we need to establish some conventions. We think of the vertices of an ideal tetrahedron τ as lying on the Riemann sphere, which is the boundary at infinity of hyperbolic 3-space \mathbb{H}^3 . By using the upper half-plane model we can identify the boundary of \mathbb{H}^3 at infinity with the Riemann sphere $\widehat{\mathbb{C}} = \mathbb{C} \cup \{\infty\}$. (This is one way to compute $\text{Isom}(\mathbb{H}^3) = \text{PSL}_2(\mathbb{C})$: isometries preserve the boundary, whose isometries are given by the group $\text{PSL}_2(\mathbb{C})$ of fractional linear transformations.) The geometry of an ideal tetrahedron Δ is determined by the locations $p_i \in \widehat{\mathbb{C}}, i = 0, 1, 2, 3$ of the points, which is summarized by their cross-ratio, in this context called a *shape parameter* $z \in \widehat{\mathbb{C}}$. One pair of edges of Δ has shape parameter z , and the others have shapes $1/(1-z)$ and $1-1/z$.

Specifying where they are determines the geometry of τ .

DEFINITION 3.3. For $p_0, p_1, p_2, p_3 \in \widehat{\mathbb{C}} = \mathbb{C} \cup \{\infty\}$, the *cross-ratio* is

$$[p_0 : p_1 : p_2 : p_3] = \frac{(p_0 - p_3)(p_1 - p_2)}{(p_0 - p_2)(p_1 - p_3)}.$$

It is well known that $[p_0 : p_1 : p_2 : p_3]$ is invariant under the action of $\text{PSL}_2(\mathbb{C})$ by fractional linear transformations.

We follow [Cho18, Definition 2.6] and use a slightly nonstandard convention on edges and shape parameters. Our tetrahedra have signs, and the relationship between the shape parameters and the cross-ratio depends on the sign. It turns out that this is much more convenient for our purposes.

⁹ Actually, three: there are also gluing equations for the internal edges of the octahedra when we divide them into tetrahedra. We will choose the shapes of the component tetrahedra so that the gluing equations of the internal edges are automatically satisfied, so we can ignore them for now.

[Cho18] J. Cho, “Quandle theory and the optimistic limits of the representations of link groups”. [arXiv](#) [DOI](#)

DEFINITION 3.4. An ideal tetrahedron is *labeled* if its vertices are totally ordered by labeling them with the set $\{0, 1, 2, 3\}$ and it is assigned a *sign* $\epsilon \in \{1, -1\}$. If the vertices of a labeled tetrahedron τ are at points $p_0, p_1, p_2, p_3 \in \widehat{\mathbb{C}}$, then we assign the edges 01 and 23 the shape parameter z^0 given by the cross-ratio

$$z^0 := [p_0 : p_1 : p_2 : p_3]^\epsilon.$$

We assign the edges 12 and 03 the shape z^1 and the edges 02 and 13 the shape z^2 given by

$$(z^1)^\epsilon = \frac{1}{1 - (z^0)^\epsilon} \text{ and } (z^2)^\epsilon = 1 - \frac{1}{(z^0)^\epsilon}.$$

A tetrahedron is *degenerate* if one (hence all of) its shape parameters is 0, 1, or ∞ .

This means that

$$z^1 = \frac{1}{1 - z^0} \quad z^2 = 1 - \frac{1}{z^0} \quad \text{for } \epsilon = 1 \quad (18)$$

$$z^1 = 1 - \frac{1}{z^0} \quad z^2 = \frac{1}{1 - z^0} \quad \text{for } \epsilon = -1 \quad (19)$$

In general, if we index tetrahedra by a symbol j , we write z_j^k for the k th shape parameter of tetrahedron j and ϵ_j for its sign. It is frequently useful to use the identity

$$z_j^{k+1} = \begin{cases} \frac{1}{1 - z_j^k} & \epsilon_j = 1 \\ 1 - \frac{1}{z_j^k} & \epsilon_j = -1 \end{cases}$$

The index k is modulo 3, so $z_j^3 = z_j^0$ regardless of ϵ_j .

3.3. The four-term decomposition

We can now describe the four-term decomposition, which we will use to show that the holonomy representation of a diagram given in Definition 2.15 agrees with the shapes of the ideal octahedra from Section 3.1. The idea is to draw a single vertical edge from P_1 to P_2 , as in Figure 16. This divides each octahedron into four tetrahedra, each of which lies between two segments of the diagram, and we label them N, S, E, W as with the regions near a crossing (see Figure 3).

To describe shapes for the tetrahedra we label them and identify their vertices with points of $\widehat{\mathbb{C}}$. At a positive crossing, our convention is that the vertices are always ordered $P_2 P_1 P_- P_+$, that τ_N and τ_S are positive, and that τ_W and τ_E are negative. (Recall that P_+, P'_+ and P_-, P'_- are identified.) Geometrically P_- is located at 0, P_+ is located at ∞ , and we vary the locations of P_1 and P_2 to give the correct shapes. At a negative crossing we flip the signs of the tetrahedra. Both sets of conventions are summarized in Tables 1 and 2.

THEOREM 3.5. At any non-pinched crossing the shaped tetrahedra of Tables 1 and 2 are geometrically non-degenerate and glue together to give an octahedron matching Definition 3.1. \diamond

Proof. The non-degeneracy claim is obvious from Definition 2.8, so consider the claim about gluing. The horizontal edges are automatic. For example, at a positive crossing the edge $P_+ P'_-$ is the 12 edge of τ_S , so it is assigned the shape

$$z_S^0 = \frac{m_2 b_2}{m_1 b_{1'}} = o_S$$

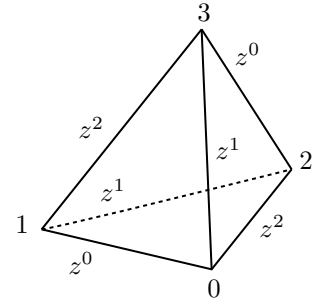


Figure 15: Shape parameters assigned to the edges of a labeled tetrahedron.

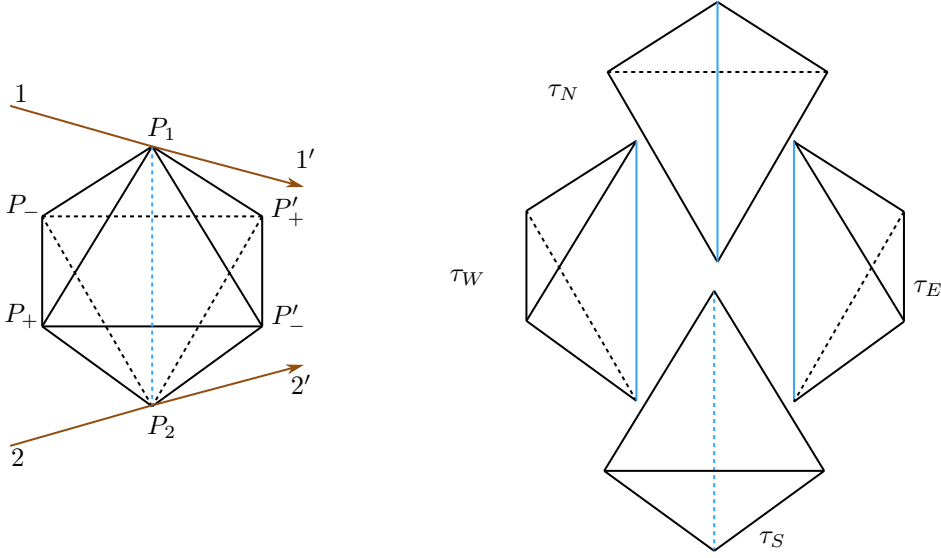


Figure 16: The four-term decomposition of an ideal octahedron at a positive crossing.

	vertices	sign ϵ	P_1	P_2	shape z^0
τ_N	$P_1 P_2 P'_- P_+$	1	$-1/b_1$	$-1/b_{2'}$	$b_{2'}/b_1$
τ_W	$P_1 P_2 P_- P_+$	-1	$-1/m_1 b_1$	$-1/b_2$	$m_1 b_1/b_2$
τ_S	$P_1 P_2 P_- P'_+$	1	$-1/m_1 b_{1'}$	$-1/m_2 b_2$	$m_2 b_2/m_1 b_{1'}$
τ_E	$P_1 P_2 P'_- P'_+$	-1	$-1/b_{1'}$	$-1/m_2 b_{2'}$	$b_{1'}/m_2 b_{2'}$

Table 1: Geometric data associated to the four-term decomposition at a positive crossing.

	vertices	sign ϵ	P_1	P_2	shape z^0
τ_N	$P_2 P_1 P'_- P_+$	-1	$-1/b_1$	$-1/b_{2'}$	$b_{2'}/b_1$
τ_W	$P_2 P_1 P_- P_+$	1	$-1/m_1 b_1$	$-1/b_2$	$m_1 b_1/b_2$
τ_S	$P_2 P_1 P_- P'_+$	-1	$-1/m_1 b_{1'}$	$-1/m_2 b_2$	$m_2 b_2/m_1 b_{1'}$
τ_E	$P_2 P_1 P'_- P'_+$	1	$-1/b_{1'}$	$-1/m_2 b_{2'}$	$b_{1'}/m_2 b_{2'}$

Table 2: Geometric data associated to the four-term decomposition at a negative crossing. The only difference from the positive case is that all the tetrahedra have the opposite sign.

as it should be.

The significant part is checking the vertical edges. Again, we compute a representative case. Consider the edge P_+P_2 at a positive crossing. Its shape has contributions from τ_W and τ_S ; from Table 1 they are

$$z_W^1 z_S^1 = \left(1 - \frac{b_2}{m_1 b_1}\right) \left(1 - \frac{m_2 b_2}{m_1 b_{1'}}\right)^{-1} = \frac{b_{1'}}{b_1} \frac{b_2 - m_1 b_1}{m_2 b_2 - m_1 b_{1'}}$$

and by Lemma 2.10 this is equal to $1/m_2 a_2 = o_2$. \square

Unfortunately, the four-term decomposition has a technical problem: at any pinched crossing (in the sense of Definition 2.8) all four tetrahedra have shape parameters $\{0, 1, \infty\}$, so they are geometrically degenerate. As shown in Example 6.4 and Section 6.3 there are plenty of interesting examples without pinched crossings, but to prove general existence theorems like Theorem 3.10 we need to use the five-term decomposition.

However, the four-term decomposition is still quite useful. We have discussed two notions of holonomy representation for a shaped diagram D of a link L :

1. The holonomy representation $\rho : \Pi_1(D) \rightarrow \mathrm{SL}_2(\mathbb{C})$ given by Definition 2.15.
2. The holonomy representation $\rho : \pi_1(M_L) \rightarrow \mathrm{PSL}_2(\mathbb{C})$ induced by the geometric data of Tables 1 and 2.

We can use the four-term decomposition to make sure that these definitions agree. To be precise about the second one, we use face pairings.

The idea is as follows: We determine the geometry of the tetrahedra in an ideal triangulation by choosing where on $\partial\mathbb{H}^3 = \widehat{\mathbb{C}}$ their ideal vertices lie. When we glue two tetrahedra together along a face, they will in general disagree about where the vertices of that face are. To fix this, we include a *face map* $g \in \mathrm{PSL}_2(\mathbb{C}) = \mathrm{Isom}(\widehat{\mathbb{C}})$ sending the vertices of one face to the other by a fractional linear transformation. Together all the face maps give a representation $\pi_1(M_L) \rightarrow \mathrm{PSL}_2(\mathbb{C})$. By carefully choosing the locations of the points P_1 and P_2 , we see that the face-pairing maps at a crossing exactly correspond to the matrices in Definition 2.15.

THEOREM 3.6. The holonomy representation of a shaped diagram agrees with the holonomy representation generated by the face maps of the associated four-term decomposition. \diamond

To prove the theorem it is helpful to consider a slightly different description of an ideal octahedron at a positive crossing related to ideal triangulations of discs.¹⁰ Every link L can be represented as the closure of a braid β . If we view β as an element of the mapping class group of the n -punctured disc D_n , then the complement M_L of L is the mapping torus¹¹ of β . If we ideally triangulate D_n and interpret the action of β in terms of this triangulation, we can get an ideal triangulation of the mapping torus of β , that is of M_L . We describe this process in Figure 17. (To visualize it, it may help to examine Figure 18.)

We start with the triangulation in Figure 17a. For simplicity we consider a single crossing at a time, so we only need to consider two punctures P_1 and P_2 (plus two auxiliary punctures P_+ at the top and P_- at the bottom.) We think of these punctures as corresponding to strands oriented out of the page.¹²

We can modify ideal triangulations by flipping the diagonal of a quadrilateral. From a 3-dimensional perspective, we are attaching the final edge of a tetrahedron above its base. In Figure 17b we add a *red* edge to build an ideal tetrahedron $P_2P_-P_+P_1$. We then add two *green* edges, building two more tetrahedra. Finally, we add the *blue* edge to finish.

¹⁰ This has something to do with cluster algebras, as discussed in Section 5.

¹¹ If $f : \Sigma \rightarrow \Sigma$ is a homeomorphism, then mapping torus of f is the space $\Sigma \times [0, 1]$ modulo the relation $(x, 0) \sim (f(x), 1)$.

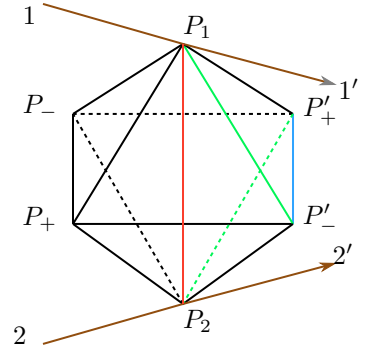


Figure 18: The edges of this octahedron are colored to match the edges in Figure 17.

¹² It's straightforward to extend this picture to any number of interior punctures by gluing copies of Figure 17a along the vertical edges.

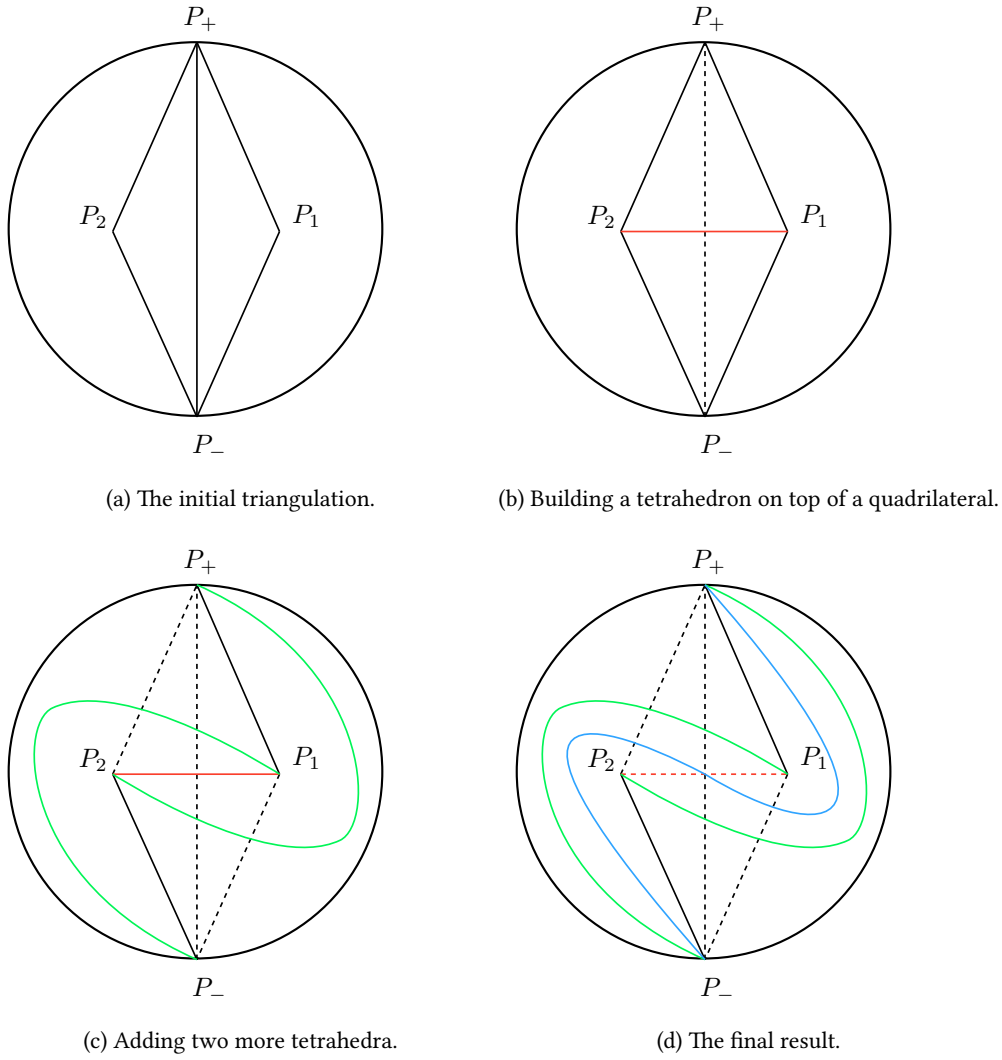


Figure 17: Building an ideal octahedron.

Ignoring the interior dashed edges, which are now below the tetrahedra we have added, we have a new, twisted copy of the triangulation in Figure 17a. By rotating P_1 above P_2 , we pull the green edges taut and obtain our original picture, but with the points P_1 and P_2 swapped. In the process, we have braided the point P_1 over the point P_2 . This corresponds to a positive braiding in our conventions, assuming that the strands are oriented out of the page in Figure 17. At the same time we have built a twisted octahedron at the crossing as required.

We are almost ready to compute the face maps, but first we need to pick a slightly unusual convention on fractional linear transformations, in order to match our convention that words in $\Pi_1(D)$ are read left-to-right.

DEFINITION 3.7. Elements of $\mathrm{PSL}_2(\mathbb{C})$ act on $\hat{\mathbb{C}}$ on the *right* by

$$z \cdot \begin{bmatrix} a & b \\ c & d \end{bmatrix} = \frac{az + c}{bz + d}.$$

LEMMA 3.8. The face maps (as elements of $\mathrm{PSL}_2(\mathbb{C})$) of the octahedron at a positive crossing agree with the holonomies assigned to the diagram complement by the shape parameters. \diamond

Proof. If we think of the face map in Figure 19 as going from τ_W to τ_N , then it represents the holonomy from travelling above strand 2, which should be mapped to χ_2^+ . Observe that for any $z \in \hat{\mathbb{C}}$,

$$z \cdot \chi_2^+ = z \cdot \begin{bmatrix} a_2 & 0 \\ (a_2 - 1/m_2)/b_2 & 1 \end{bmatrix} = a_2 z + \frac{a_2}{b_2} - \frac{1}{m_2 b_2}.$$

In particular, we see that χ_2^+ fixes ∞ , maps $-1/b_2$ to $-1/m_2 b_2$, and maps $-1/m_1 b_1$ to

$$(-1/m_1 b_1) \cdot \chi_2^+ = a_2 \left(\frac{1}{b_2} - \frac{1}{m_1 b_1} \right) - \frac{1}{m_2 b_2} = -\frac{1}{m_1 b_1'}.$$

Because fractional linear transformations are totally determined by their action on three points of $\hat{\mathbb{C}}$, we conclude that the face map agrees with χ_2^+ .

The negative holonomy of strand 2 does not correspond directly to a face map, but the face map going from τ_W to τ_N similarly corresponds to the *inverse* negative holonomy of χ_1 . We see that the transformation

$$z \cdot (\chi_1^-)^{-1} = z \cdot \begin{bmatrix} 1 & -(1 + m_1/a_1)b_1 \\ 0 & 1/a_1 \end{bmatrix} \left(-b_1 - \frac{m_1 b_1}{a_1} + \frac{1}{z a_1} \right)^{-1}$$

preserves 0, maps $1/m_1 b_1$ to $-1/b_1$, and maps $-1/m_2 b_2$ to

$$(-1/m_2 b_2) \cdot g^-(\chi_1)^{-1} = \left(-b_1 - \frac{m_1 b_1}{a_1} - \frac{b_2}{a_1} \right)^{-1} = -\frac{1}{b_2'}.$$

There is a parallel characterization of the holonomies on the other side of the crossing. For example, $\chi_{2'}^+$ corresponds to the gluing map between τ_N and τ_E , and correspondingly acts on the vertices of τ_N by

$$\begin{aligned} \infty \cdot \chi_{2'}^+ &= \infty \\ (-1/b_{2'}) \cdot \chi_{2'}^+ &= -1/m_2 b_{2'} \\ (-1/b_1) \cdot \chi_{2'}^+ &= -\frac{a_{2'}}{b_1} + \frac{a_{2'}}{b_{2'}} - \frac{1}{m_2 b_{2'}} = -1/b_{1'}, \end{aligned}$$

and similarly the face map gluing τ_S to τ_E is $(\chi_{1'}^-)^{-1}$. \square

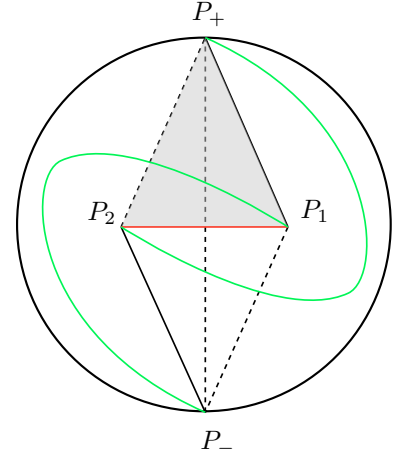


Figure 19: The face corresponding to χ_2^+ .

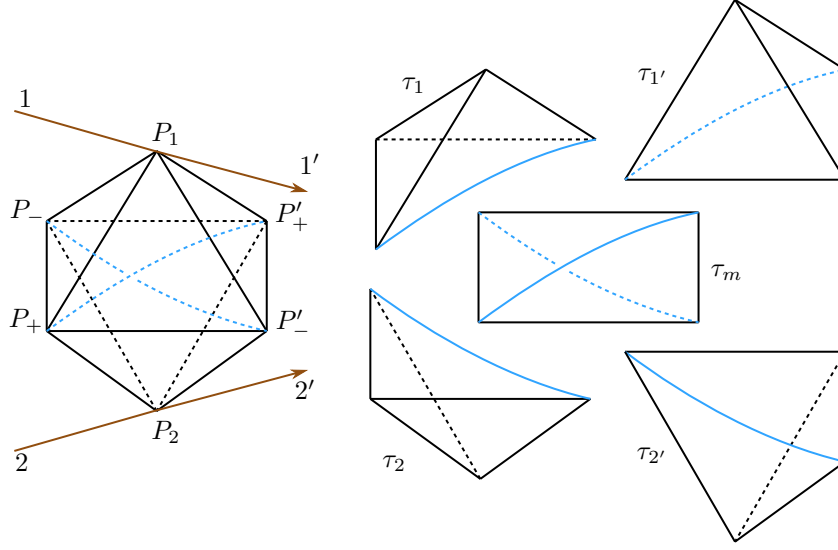


Figure 20: Decomposition of the octahedron at a positive crossing into five tetrahedra.

	vertices	sign ϵ	shape z^0
τ_1	$P_1 P_- P_+ P'_+$	1	a_1/m_1
τ_2	$P_2 P_+ P_- P'_-$	1	$1/m_2 a_2$
$\tau_{1'}$	$P_1 P'_- P_+ P'_+$	-1	$m_1/a_{1'}$
$\tau_{2'}$	$P_2 P'_+ P_- P'_-$	-1	$m_2 a_{2'}$
τ_m	$P_- P'_- P_+ P'_+$	1	$a_{1'}/a_1$

Table 3: Geometric data for the five-term decomposition at a positive crossing.

Proof of Theorem 3.6. The theorem is a corollary of the previous lemma. At a positive crossing, we have shown the matrices χ_2^+ , χ_1^- , χ_2^+ , and χ_1^- agree with the corresponding face maps. χ_2^- is now the *unique* matrix of the form

$$\begin{bmatrix} 1 & * \\ 0 & * \end{bmatrix}$$

such that

$$\text{tr } \chi_2^+(\chi_2^-)^{-1} = m_2 + m_2^{-1} \text{ and } \det \chi_2^+(\chi_2^-)^{-1} = 1,$$

and similarly for the other strands. This shows that we have agreement at any positive crossing. By repeating the computation in Lemma 3.8 for negative crossings we obtain the theorem. \square

3.4. The five-term decomposition

We can divide the octahedron at a crossing into five tetrahedra, as in Figure 20. We think of this decomposition as being associated to the a -variables. We record the geometric data of the tetrahedra in Table 3.

PROPOSITION 3.9. At any non-degenerate crossing the shaped tetrahedra of Tables 3 and 4 are non-degenerate and glue together to give an octahedron matching Definition 3.1. \diamond

	vertices	sign ϵ	shape z^0
τ_1	$P_1 P_+ P_- P'_-$	-1	$1/a_1 m_1$
τ_2	$P_2 P_- P_+ P'_+$	-1	a_2/m_2
$\tau_{1'}$	$P_1 P'_+ P_- P'_-$	1	$m_1 a_{1'}$
$\tau_{2'}$	$P_2 P'_- P_+ P'_+$	1	$m_2/a_{2'}$
τ_m	$P_- P'_- P_+ P'_+$	-1	$a_1/a_{1'}$

Table 4: Geometric data for the five-term decomposition at a negative crossing.

Proof. We first check the non-degeneracy claim. A crossing is non-degenerate if $a_1/a'_1 = a_2/a_{2'}$ is not equal to 1, which is the same as saying that τ_m is geometrically non-degenerate. Suppose the crossing is positive. Then since

$$\frac{a_1}{a_{1'}} = 1 - \frac{m_1 b_1}{b_2} \left(1 - \frac{a_1}{m_1}\right) \left(1 - \frac{1}{m_2 a_2}\right) \neq 1$$

we cannot have $a_1 = m_1$ or $a_2 = 1/m_2$, which says that τ_1 and τ_2 are geometrically non-degenerate. There is a similar expression for $a_1/a_{1'}$ in terms of $a_{1'}, a_{2'}, b_{1'}$, and $b_{2'}$ which comes from inverting the map B , and it shows that $a_1/a_{1'} \neq 1$ implies $a_{1'} \neq m_1$ and $a_{2'} \neq 1/m_2$, so $\tau_{1'}$ and $\tau_{2'}$ are geometrically non-degenerate. If the crossing is negative, a similar argument shows that $a_1/a_{1'} \neq 1$ implies $a_1, a_{1'} \neq 1/m_1$ and $a_2, a_{2'} \neq m_2$.

Now we check the gluing relations. In contrast to before, the vertical edges are automatic. For example, at a positive crossing the total shape of $P_- P_1$ should be $o_1 = a_1/m_1$, and the only contributing tetrahedron is τ_1 :

$$z_1^0 = \frac{a_1}{m_1} = o_1.$$

The horizontal edges require using some identities on $a_1/a_{1'} = a_{2'}/a_2$. As always, we compute some representative examples. Consider the edge $P_- P_+$ at a positive crossing, which should have shape $o_{12} = b_2/m_1 b_1$. It has contributions from τ_1, τ_2 , and τ_m , which give a shape

$$z_1^1 z_2^1 z_m^2 = \left(1 - \frac{a_1}{m_1}\right)^{-1} \left(1 - \frac{1}{m_2 a_1}\right)^{-1} \left(1 - \frac{a_1}{a_{1'}}\right)$$

By Definition 2.4,

$$1 - \frac{a_1}{a_{1'}} = \frac{m_1 b_1}{b_2} \left(1 - \frac{a_1}{m_1}\right) \left(1 - \frac{1}{m_2 a_2}\right)$$

so we see that

$$z_1^1 z_2^1 z_m^2 = \frac{m_1 b_1}{b_2} = o_W.$$

Similarly, at a positive crossing the edge $P'_- P'_+$ has contributions from $\tau_{1'}, \tau_{2'}$, and τ_m , which give a shape

$$z_{1'}^1 z_{2'}^1 z_m^2 = \left(1 - \frac{m_1}{a_{1'}}\right)^{-1} (1 - m_2 a_{2'})^{-1} \left(1 - \frac{a_1}{a_{1'}}\right).$$

By using the inverse B^{-1} of the braiding we can compute that

$$1 - \frac{a_1}{a_{1'}} = \frac{b_{1'}}{m_2 b_{2'}} \left(1 - \frac{m_1}{a_{1'}}\right) (1 - m_2 a_{2'})$$

and we conclude that

$$z_1^1 z_2^1 z_m^2 = \frac{b_{1'}}{m_2 b_{2'}} = o_E. \quad \square$$

While the five-term decomposition uses more tetrahedra, it has a nice nondegeneracy property:

THEOREM 3.10. Let ρ be a $\mathrm{SL}_2(\mathbb{C})$ -structure on a link L . We say ρ is *meridian-trivial* if $\rho(m) = \pm 1$, that is if sends any meridian of L to plus or minus the identity matrix. If ρ is meridian-nontrivial, then for any diagram D of L there is a shaping of D such that:

1. the holonomy representation of D is conjugate to ρ , and
2. all the tetrahedra in the five-term decomposition associated to D are geometrically nondegenerate. \diamond

Proof. This is due to Yoon, who adapted a result of Cho [Cho16]. As discussed in Section 6.2 we can solve for non-degenerate shapings in terms of only the variables a_i and m_i . Using the region variables instead of the a_i , such solutions are exactly the “non-degenerate points” of [Yoo21], so the claim is Theorem 1.2 of [Yoo21]. \square

4. DECORATED REPRESENTATIONS

It turns out that our coordinates do not just describe a representation $\rho : \pi_1(S^3 \setminus L) \rightarrow \mathrm{SL}_2(\mathbb{C})$, but actually give slightly more information called a *decoration*. These show up naturally in a few contexts: some indeterminacies in the A -polynomial come from a choice of decoration,¹³ and decorations occur naturally in Ptolemy coordinates and the computation of complex volume.

In this section we discuss decorations, then explain how to compute them from shaping of a link diagram. In particular we show how to compute the longitude eigenvalues of the holonomy representation.

4.1. Peripheral subgroups and decorations

DEFINITION 4.1. For a link L in S^3 the *exterior* $E(L) := S^3 \setminus \nu(L)$ is the complement of an open regular neighborhood of L . It is a compact manifold with boundary $\partial E(L) = T_1 \amalg \cdots \amalg T_n$ a disjoint union of tori, one for each component of L . We call the image $H_j \subset \pi_1(S^3 \setminus L)$ of $\pi_1(T_j)$ the *peripheral subgroup* associated to the component L_j .

Each H_j is isomorphic to \mathbb{Z}^2 . The usual choice of generators are a *meridian* m_j and *longitude* l_j . (An example is given in Figure 21.) Unless noted we always use the zero-framed longitude.

Because H_j is abelian we can always conjugate ρ so that $\rho(m_j)$ and $\rho(l_j)$ are both lower-triangular. Another way to say this is that we can always identify $\rho(H_j)$ with a subgroup of B , where $B \subset \mathrm{SL}_2(\mathbb{C})$ is the subgroup of lower-triangular matrices.

DEFINITION 4.2. A *decoration* [GTZ15, Section 4] of $\rho : \pi_1(S^3 \setminus L) \rightarrow \mathrm{SL}_2(\mathbb{C})$ is a choice of identification of each peripheral $\rho(H_j)$ with a subgroup of B .

Strictly speaking we are using the characterization of decorations up to equivalence given in [GTZ15, Proposition 4.6]. The choice to use lower-triangular matrices is nonstandard but it matches our conventions in Definition 3.7.

[Cho16] J. Cho, “Optimistic limit of the colored Jones polynomial and the existence of a solution”. [arXiv](#) [DOI](#)

[Yoo21] S. Yoon, “On the potential functions for a link diagram”. [arXiv](#) [DOI](#)

¹³ The A -polynomial is usually described as a Laurent polynomial in two variables m and ℓ that is well-defined up to simultaneous inversion $m \mapsto m^{-1}$, $\ell \mapsto \ell^{-1}$. These variables represent the meridian and longitude eigenvalues determined by the decorated representation and the inversion comes from changing the choice of decoration.

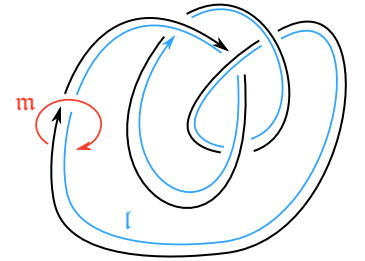


Figure 21: A meridian m (in red) and longitude l (in blue) for the figure-eight knot.

[GTZ15] S. Garoufalidis, D. P. Thurston, and C. K. Zickert, “The complex volume of $\mathrm{SL}(n, \mathbb{C})$ -representations of 3-manifolds”. [arXiv](#) [DOI](#)

REMARK 4.3. A decoration determines preferred eigenvalues m_j of each $\rho(\mathfrak{m}_j)$ and ℓ_j of each $\rho(\mathfrak{l}_j)$, because we identify them with matrices

$$\rho(\mathfrak{m}_j) \sim \begin{pmatrix} m_j & 0 \\ * & m_j^{-1} \end{pmatrix}, \quad \rho(\mathfrak{l}_j) \sim \begin{pmatrix} \ell_j & 0 \\ * & \ell_j^{-1} \end{pmatrix}$$

Conversely, when $m_j \neq \pm 1$ the choice of m_j versus m_j^{-1} determines a decoration. In the boundary-parabolic case $m_j = \pm 1$ the correspondence is more complicated: we have

$$\rho(\mathfrak{m}_j) \sim \pm \begin{pmatrix} 1 & 0 \\ 1 & 1 \end{pmatrix}, \quad \rho(\mathfrak{l}_j) \sim \begin{pmatrix} \epsilon & 0 \\ c & \epsilon \end{pmatrix}$$

where $\epsilon \in \{1, -1\}$ and $c \in \mathbb{C}$ is the *cuspidal shape*.

More generally a decoration gives a choice $\delta(x)$ of eigenvalue of $\rho(x)$ for every $x \in \pi_1(T_j)$, since

$$\rho(x) \text{ is conjugate to } \begin{pmatrix} \delta(x) & 0 \\ * & \delta(x)^{-1} \end{pmatrix}$$

Another way to phrase this is to say that ρ induces a homomorphism

$$\rho : H_1(\partial M; \mathbb{Z}) = \bigoplus_{j=1}^n H_1(T_j; \mathbb{Z}) \rightarrow \mathrm{SL}_2(\mathbb{C}).$$

and a decoration gives lift

$$\delta : H_1(\partial M; \mathbb{Z}) \rightarrow \mathbb{C}^\times.$$

We sometimes call δ an *eigenvalue decoration* because it is almost but not quite a decoration: when our representation is boundary-parabolic we also need to know the cuspidal shape to determine one. Cuspidal shapes can be computed from the octahedral decomposition [KKY19, Section 5.1] with a similar method but we are most interested in δ . Our main result in this section is an explicit formula for it in terms of a diagram shaping.

THEOREM 4.4. Let D be a diagram of a link L . A shaping χ of D determines an eigenvalue decoration $\delta = \delta_\rho$ of its holonomy representation ρ . Explicitly, the homomorphism δ is given by

$$\delta(\mathfrak{m}_j) = m_j \tag{20}$$

$$\delta(\mathfrak{l}_j) = m_j^{-w_j} \prod_k b_k^{\eta_k} \tag{21}$$

where w_j is the writhe of component j , the product is over all segments in component j , and

$$\eta_k := \begin{cases} 1 & \text{if segment } k \text{ is over-under,} \\ -1 & \text{if it is under-over, and} \\ 0 & \text{otherwise.} \end{cases} \quad \diamond$$

We typically do not work directly with the matrices of the holonomy to determine the decoration. Instead, we use a more geometric characterization. Thinking of the boundary torus T_j of $E(L)$ as the boundary of a cusp it has an affine structure locally modeled on the Euclidean plane \mathbb{C} . The holonomy acts by affine transformations, and the eigenvalues m_j, ℓ_j are related to the scaling factors of these transformations. We refer to [Pur20, Section 4.3] for a

[KKY19] H. Kim, S. Kim, and S. Yoon, *Octahedral developing of knot complement II: Ptolemy coordinates and applications*. [arXiv](#)

general discussion and [KKY18, Section 4] for more details in the context of the octahedral decomposition.

This perspective lets us compute the holonomies directly from an ideal triangulation of $S^3 \setminus L$. By truncating our tetrahedra we get a triangulation of the cusps and we can read off the eigenvalues in terms of the shapes.

DEFINITION 4.5. Let γ be an oriented simple curve in the boundary T of a cusp of $E(L)$, which we triangulate by truncating an ideal triangulation of $S^3 \setminus L$. Isotope γ so it intersects only edges of the triangulation transversely and cuts a single corner off of each triangle. This corner is associated to the edge of an ideal tetrahedron, and we assign it the shape parameter z_k of that edge. The *holonomy* of γ is

$$\text{Hol}(\gamma) := \prod_{k=1}^n z_k^{\epsilon_k}$$

where the product is over all the triangles γ passes through,

$$\epsilon_k = \begin{cases} +1 & \text{if the corner is right of } \gamma, \\ -1 & \text{if the corner is left of } \gamma, \end{cases}$$

and we view the boundary triangles from outside $S^3 \setminus L$.¹⁴ We give an example in Figure 22.

For the octahedral decomposition this triangulation comes from squares, which are subdivided in different ways depending on whether we use the four-term or five term-decomposition. In the rest of this section we compute the holonomy of the meridian and longitude using this construction, which along with the next proposition gives a proof of Theorem 4.4.

PROPOSITION 4.6. Consider an ideal triangulation of $S^3 \setminus L$ with a shaping corresponding to the representation $\rho : \pi_1(S^3 \setminus L) \rightarrow \text{SL}_2(\mathbb{C})$. The holonomy map Hol of the triangulation gives a homomorphism

$$\text{Hol} : H_1(\partial E(L); \mathbb{Z}) \rightarrow \mathbb{C}^\times$$

and any decoration of $S^3 \setminus L$ satisfies

$$\delta(x)^2 = \text{Hol}(x) \text{ for all } x \in H_1(\partial E(L); \mathbb{Z}).$$

◇

Proof. The square root comes from the difference between the action of \mathbb{C}^\times on \mathbb{C} by multiplication and the action of $\text{SL}_2(\mathbb{C})$ by fractional linear transformations. Geometrically, the holonomy $\text{Hol}(x)$ represents a scaling/rotation of \mathbb{C} by multiplication by an element of \mathbb{C}^\times . On the other hand we can also compute this action directly from the matrix $\rho(x) \in \text{SL}_2(\mathbb{C})$. Using the decoration δ , $\rho(x)$ is conjugate to

$$\tilde{\rho}(x) = \begin{pmatrix} \delta(x) & 0 \\ b & \delta(x)^{-1} \end{pmatrix}$$

for some $b \in \mathbb{C}$ and (following Definition 3.7)

$$\tilde{\rho}(x) \cdot z = \frac{\delta(x)z + b}{\delta(x)^{-1}} = \delta(x)^2 z + b\delta(x)^{-1}$$

We are interested only in the scaling action $\delta(x)^2$, which is the *square* of the eigenvalue $\delta(x)$ as claimed. \square

¹⁴ This is the opposite of the usual convention, which corresponds to our choice in Definition 3.7.

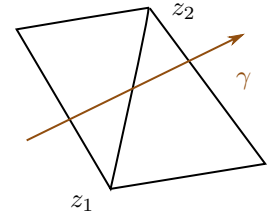


Figure 22: A curve γ in the boundary triangulation, viewed from *outside* the manifold. We assign it the holonomy $\text{Hol}(\gamma) = z_1 z_2^{-1}$.

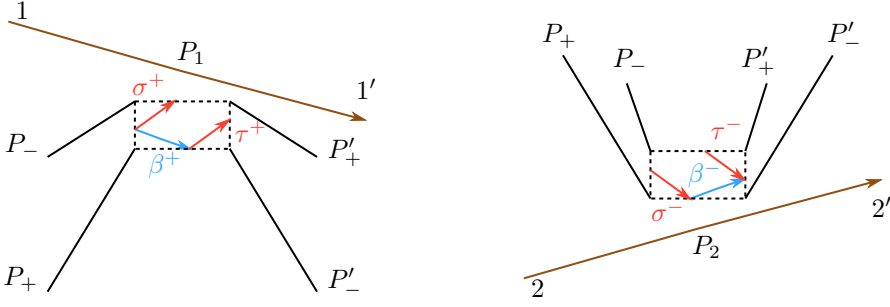


Figure 23: Curves in the boundary of the octahedral decomposition near a positive crossing.

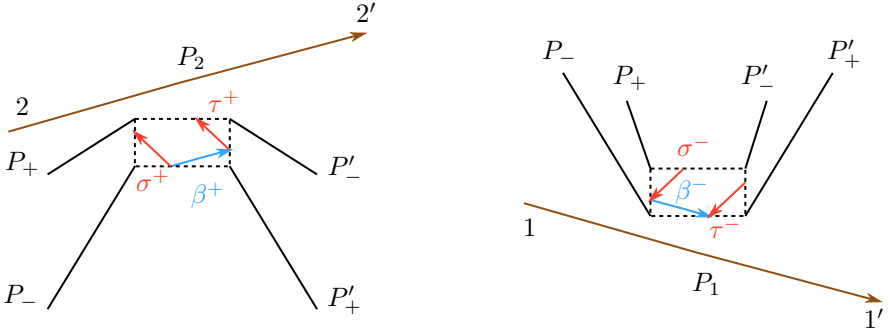


Figure 24: Curves in the boundary of the octahedral decomposition near a negative crossing.

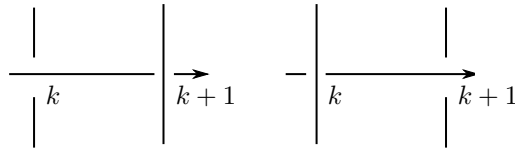
For a $\mathrm{PSL}_2(\mathbb{C})$ representation the eigenvalues $\delta(x)$ are only determined up to sign, so knowing Hol determines δ . For $\mathrm{SL}_2(\mathbb{C})$ representations it is not obvious how to choose the sign of $\sqrt{\mathrm{Hol}}$; we discuss this further in Remark 4.12.

This can be somewhat subtle: for a boundary-parabolic representation we can always choose a lift where the meridians have trace 2, but the longitudes might still have trace -2 . This is related to the *obstruction class* of the representation [CYZ20, Section 2.1].

4.2. The meridians

We first compute the holonomy of the meridian \mathfrak{m} of a segment of a shaped diagram. We already know that the answer should be m^2 when the segment is assigned the shape (a, b, m) , so our goal is to check this against the geometry. We can express \mathfrak{m} as a composition of the curves σ^\pm, τ^\pm shown in Figure 23. The exact form depends on the type of segment:

PROPOSITION 4.7. Consider a segment between crossings labeled k and $k+1$. Using the segment

Figure 25: An over-under (left) and under-over (right) segment between crossings k and $k+1$.

types in Figure 25,

$$\begin{aligned} \tau_k^+ \sigma_{k+1}^- &= \mathbf{m} && \text{at an over-under segment,} \\ \tau_k^- \sigma_{k+1}^+ &= \mathbf{m} && \text{at an under-over segment, and} \\ \tau_k^\pm &= \sigma_{k+1}^\pm && \text{at an over-over or under-under segment.} \end{aligned}$$

where \mathbf{m} is the meridian of the segment. \diamond

Proof. We can see this directly by composing the curves in Figures 23 and 24 during the gluing. Alternately, it follows from the discussion in [KKY18, Section 4.1] and in particular [KKY18, eq. 10]. Notice that their meridians are the inverse of ours. \square

Now we can read off the holonomy of the curves directly from the cusp triangulation:

LEMMA 4.8. At a positive crossing,

$$\begin{aligned} \text{Hol}(\sigma^+) &= o_1^{-1} = \frac{m_1}{a_1} && \text{Hol}(\tau^+) = o_{1'} = \frac{m_1}{a_{1'}} \\ \text{Hol}(\sigma^-) &= o_2^{-1} = m_2 a_2 && \text{Hol}(\tau^-) = o_{2'} = m_2 a_{2'} \end{aligned}$$

while at a negative crossing

$$\begin{aligned} \text{Hol}(\sigma^+) &= o_2^{-1} = \frac{m_2}{a_2} && \text{Hol}(\tau^+) = o_{2'} = \frac{m_2}{a_{2'}} \\ \text{Hol}(\sigma^-) &= o_1^{-1} = m_1 a_1 && \text{Hol}(\tau^-) = o_{1'} = m_1 a_{1'} \end{aligned}$$

where the o_j are the shapes of the vertical edges given in equations (14) and (16). \diamond

Proof. To apply Definition 4.5 we divide the squares of Figure 26 into triangles by dividing our octahedra into tetrahedra. Using the five-term decomposition this looks like Figure 26, and then at a positive crossing we have

$$\text{Hol}(\sigma^+) = (z_1^0)^{-1} \frac{m_1}{a_1}$$

and

$$\text{Hol}(\sigma^-) = (z_W^1)^{-1} (z_S^1)^{-1} = (z_1^0)^{-1} = m_2 a_2$$

because we view the boundary from outside the link exterior. The other cases follow from similar computations. \square

Proof of equation (20). Consider a segment assigned the shape $\chi = (a, b, m)$ between crossings k and $k+1$. If it is an over-under segment, then

$$\text{Hol}(\mathbf{m}) = \text{Hol}(\tau_k^+ \sigma_{k+1}^-) = \frac{m}{a} m a = m^2$$

as claimed. Notice that this computation does not rely on the signs of the crossings. Similarly at an under-over segment we have

$$\text{Hol}(\mathbf{m}) = \text{Hol}(\tau_k^- \sigma_{k+1}^+) = m a \frac{m}{a} = m^2.$$

Taking the square root gives equation (20). We know that m (and not $-m$) is the right sign because we can explicitly check that it is an eigenvalue of (13).¹⁵ We only need to check equation (20) for one segment of each link component, and at least one segment of any component of any link diagram is either over-under or under-over. (Actually, this is only true if the component has at least one crossing. By adding kinks we can always assume this.) \square

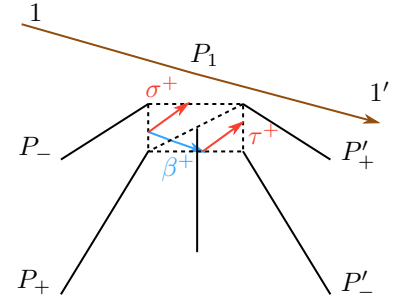


Figure 26: Subdividing using the five-term decomposition to get a triangulation of the boundary.

¹⁵ Actually, we didn't really need to go through this whole derivation using boundary holonomies: we could have just used this argument. However, it's a good warm-up for the longitude computation.

The equations for $\text{Hol}(\mathbf{m})$ are examples of m -hyperbolicity equations:

DEFINITION 4.9. The *m -hyperbolicity equation* for a segment is

$$\frac{o'}{o} = \begin{cases} m^2 & \text{if the segment is over-under or under-over, and} \\ 1 & \text{otherwise.} \end{cases}$$

where o is the shape of the vertical edge at the start of the segment and o' is the shape of the vertical edge at the end.

We just showed that when using shape coordinates the m -hyperbolicity equations automatically hold. As discussed in the proof of Theorem 3.2 they imply the gluing equations for the vertical edges.

4.3. The longitudes

Our convention is to obtain the blackboard-framed longitude $\tilde{\mathbf{l}}$ by pushing off to the right, so it is given by

$$\tilde{\mathbf{l}} = \prod_k \beta_k^{\eta_k} \quad (22)$$

where η_k is $+$ at an overcrossing and $-$ at an undercrossing and the product is over all intersections of our component with the rest of the diagram. In general the zero-framed longitude is

$$\mathbf{l} = \tilde{\mathbf{l}} - w\mathbf{m} \quad (23)$$

where w is the writhe of the link component we are considering.

EXAMPLE 4.10. In Figure 27 the blue curve is $\tilde{\mathbf{l}}$, so it is given by

$$\tilde{\mathbf{l}} = \beta_1^- \beta_2^+ \beta_3^- \beta_1^+ \beta_2^- \beta_3^+.$$

Notice that a crossing can appear twice in the product in equation (22), and for knots they always do. The zero-framed longitude is $\mathbf{l} = \tilde{\mathbf{l}} - 3\mathbf{m}$ because this diagram has writhe 3.

LEMMA 4.11. At a positive crossing

$$\begin{aligned} \text{Hol}(\beta^+) &= a_2 \frac{b_{1'}}{b_1} \\ \text{Hol}(\beta^-) &= \frac{1}{a_{1'}} \frac{b_2}{b_{2'}} \end{aligned}$$

and at a negative crossing

$$\begin{aligned} \text{Hol}(\beta^+) &= \frac{1}{a_{1'}} \frac{b_{2'}}{b_2} \\ \text{Hol}(\beta^-) &= a_2 \frac{b_1}{b_{1'}} \end{aligned}$$

Proof. For β^+ at a positive crossing, we can use the five-term decomposition as before to compute

$$\text{Hol}(\beta^+) = z_1^1 z_{1'}^1 = \left(1 - \frac{a_1}{m_1}\right)^{-1} \left(1 - \frac{a_{1'}}{m_1}\right) = a_2 \frac{b_{1'}}{b_1}$$

using equation (7). The other computations follow similarly. \square

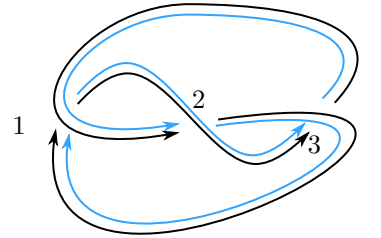


Figure 27: Here the blue curve is the blackboard-framed longitude $\tilde{\mathbf{l}}$.

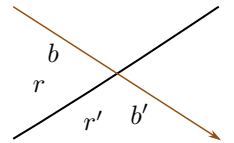


Figure 28: Following the gold strand, this crossing contributes a factor of $(r'/r)(b'/b)^\eta$ to the longitude holonomy $\text{Hol}(\mathbf{l})$.

Proof of equation (21). We can now compute $\text{Hol}(\tilde{l})$ and thus $\text{Hol}(l)$ as a product over the crossings of our diagram. To prove our claim it suffices to show that this product is the square of the right-hand-side of equation (21).

The expressions in Lemma 4.11 follow a simple pattern in terms of the *region variables* of Section 6.2. The idea is to assign variables r_k to the regions of the diagram so ratios of adjacent region variables give the a -variable of the strand between them, as in Figure 30. It is easy to see (Lemma 6.7) we can always assign region variables to any shaped diagram.

Once we do this we can summarize Lemma 4.11 by saying that the contribution of the crossing in Figure 28 is

$$\frac{r'}{r} \left(\frac{b'}{b} \right)^\eta \quad (24)$$

where η is 1 if the gold strand passes over the black strand and -1 if it passes under. The variables r, r' and b, b' correspond to the regions and segments adjacent to the crossing. We can prove equation (24) by a trivial case-by-case check, as usual.

Now we need to translate our product over crossings into a product over segments. First consider an over-under segment, like in Figure 29. The crossings at each end contribute a factor

$$a \left(\frac{b_1}{b_0} \right)^{+1} \cdot \frac{1}{a'} \left(\frac{b_2}{b_1} \right)^{-1} = \frac{r_1}{r_0} \frac{b_1}{b_0} \frac{r_2}{r_1} \frac{b_1}{b_2} = \frac{r_2}{r_0} \frac{1}{b_0 b_2} b_1^2$$

to $\text{Hol}(\tilde{l})$. In particular, we see that r_1 does not contribute, and the exponent of b_1 is $+2$. If instead we had an over-over segment, the contribution would be

$$\frac{r_1}{r_0} \frac{b_1}{b_0} \frac{r_2}{r_1} \frac{b_2}{b_1} = \frac{r_2}{r_0} \frac{b_2}{b_0}$$

and b_1 does not appear at all.

More generally, when following a component of a link diagram, the region variables appear as a telescoping product

$$\frac{r_0}{r_1} \frac{r_1}{r_2} \dots \frac{r_n}{r_0} = 1$$

and the b -variables only show up with even exponents: $+2$ if their segment is over-under, -2 if it is under-over, and 0 otherwise. We have shown that when we write $\text{Hol}(\tilde{l})$ as a product over segments,

$$\text{Hol}(\tilde{l}) = \prod_k b_k^{2\sigma_k}$$

so

$$\text{Hol}(l) = m^{-2w_j} \prod_k b_k^{2\sigma_k} = \delta(l)^2. \quad \square$$

It remains only to show that we have taken the correct sign of $\sqrt{\text{Hol}(l)}$. (We have already showed that we picked the right sign of $\sqrt{\text{Hol}(m)}$ because m is an eigenvalue of (13), not $-m$.)

REMARK 4.12. When ρ is a boundary-parabolic $\text{PSL}_2(\mathbb{C})$ -representation $\text{Hol}(m) = (\pm 1)^2 = 1$, so $\delta(m) = \pm 1$. Because the meridians generate $\pi_1(E(L))$ we can always lift ρ to $\text{SL}_2(\mathbb{C})$ by picking a sign of the meridians, say $\delta(m) = 1$. However, in general the sign of $\delta(l)$ can be -1 , regardless of the choice of lift. In fact, for a hyperbolic knot complement we have $\delta(l) = -1$ for any lift of the geometric representation [Cal06, Corollary 2.4].

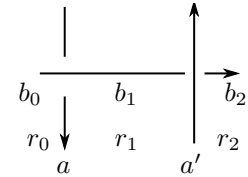


Figure 29: Region and segment variables contributing to the longitude.

We can think of this as an obstruction to lifting ρ to a boundary-unipotent $\mathrm{SL}_2(\mathbb{C})$ -representation, and in this context $\delta(\mathfrak{l}) \in \{1, -1\}$ is called the *obstruction class* [GTZ15; KKY19] of the representation. Determining the sign of $\delta(\mathfrak{l}) = \sqrt{\mathrm{Hol}(\mathfrak{l})}$ is closely related to these obstruction classes.

Proof of Theorem 4.4. The trick is again to work with a triangulation of the boundary, just as for Hol , but this time with matrices instead of elements of \mathbb{C}^\times . This is done in detail in the boundary-parabolic case in [KKY19, Section 4]; the general argument follows by extending their work to *deformed Ptolemy varieties*, as in [Yoo18, Section 2]. We sketch the idea below.

We want to encode the restriction $\rho|_{H_j}$ of ρ to the peripheral subgroup H_j of our boundary component in terms of a cocycle $N^1 \rightarrow B$, where by N^1 we mean the 1-skeleton of the triangulation of the boundary $\partial E(L)$. It turns out this gives a particularly nice description of ρ on all of M in terms of a *natural cocycle* $\mathcal{B} : M^1 \rightarrow \mathrm{SL}_2(\mathbb{C})$ on the 1-skeleton of our triangulation of $E(L)$, and we can then read off $\delta(\mathfrak{l})$ directly.

It is easy to express \mathcal{B} using the b -variables, and we get an expression for the longitude just like the ones for $\mathrm{Hol}(\beta^\pm)$. (Compare the formula $\sigma(c_i) = z_a/z_c$ in [KKY19, Section 4] to equation (24).) Once we do this it is clear that equation (21) has the correct sign. \square

5. A CONNECTION TO QUANTUM GROUPS

The shape coordinates (Section 2) are deeply related to the hyperbolic geometry of the knot complement (Section 3). However, they were originally discovered in the context of quantum groups, specifically the representation theory of quantum \mathfrak{sl}_2 . When q is a root of unity the braiding of the quantum group has some unusual properties, and understanding them leads directly to the braiding given in Definition 2.4. To obtain the geometrically interesting shape coordinates we use a presentation of $\mathcal{U}_\xi(\mathfrak{sl}_2)$ in terms of a quantum Weyl algebra. This presentation is derived from cluster algebras associated to the ideal triangulation in Figure 17a. While most of this story has either previously appeared in the literature or in the author's thesis [McP21], in this section we give a brief overview for non-specialists.

5.1. Quantum groups at roots of unity

For any simple Lie algebra \mathfrak{g} , the *quantum group* $\mathcal{U}_q(\mathfrak{g})$ is a q -analogue of the universal enveloping algebra of \mathfrak{g} . Quantum groups have a number of interesting algebraic properties; the most important for topology is the existence of an element $\mathbf{R} \in \mathcal{U}_q(\mathfrak{g}) \otimes \mathcal{U}_q(\mathfrak{g})$ called the *universal R-matrix*. It satisfies braid relations that are the key ingredient for constructing quantum invariants of knots and links [RT90; Oht01]. This construction is universal in the sense that any choice of $\mathcal{U}_q(\mathfrak{g})$ -module V determines a link invariant. For example, if we choose $\mathfrak{g} = \mathfrak{sl}_2$ and V the irreducible N -dimensional representation of $\mathcal{U}_q(\mathfrak{sl}_2)$ we get the N th colored Jones polynomial.

When q is not a root of unity, the representation theory of $\mathcal{U}_q(\mathfrak{g})$ is quite similar to the classical representation theory of \mathfrak{g} . However, at a root of unity things become much more complicated and depend on exactly which form of the quantum group we use. For the *Kac-de Concini form* [DKP91] of the quantum group, this is because the center gets much larger. We can make this precise as follows:

THEOREM 5.1. When $q = \xi$ is a primitive $2N$ th root of unity, $\mathcal{U}_\xi(\mathfrak{sl}_2)$ contains a large central subalgebra $\mathcal{Z}_0 \subset \mathcal{U}_\xi(\mathfrak{sl}_2)$. Because \mathcal{Z}_0 is a commutative Hopf algebra, we can interpret it as

[Yoo18] S. Yoon, *The volume and Chern-Simons invariant of a Dehn-filled manifold*. [arXiv](#) [DOI](#)

[RT90] N. Y. Reshetikhin and V. G. Turaev, "Ribbon graphs and their invariants derived from quantum groups". [DOI](#)

[Oht01] T. Ohtsuki, *Quantum Invariants*. [DOI](#)

[DKP91] C. De Concini, V. G. Kac, and C. Procesi, "Representations of quantum groups at roots of 1"

the algebra of functions on an algebraic group, in this case the group

$$\mathrm{SL}_2(\mathbb{C})^* = \left\{ \left(\begin{bmatrix} \kappa & 0 \\ \phi & 1 \end{bmatrix}, \begin{bmatrix} 1 & \epsilon \\ 0 & \kappa \end{bmatrix} \right) \middle| \kappa \neq 0 \right\}.$$

Concretely, characters (i.e. algebra homomorphisms) $\chi : \mathcal{Z}_0 \rightarrow \mathbb{C}$ give points of $\mathrm{SL}_2(\mathbb{C})^*$, and the product is given by

$$(\chi_1 \cdot \chi_2)(x) := (\chi_1 \otimes \chi_2)(\Delta(x))$$

where Δ is the coproduct of $\mathcal{U}_\xi(\mathfrak{sl}_2)$. The algebra \mathcal{Z}_0 is large in the sense that $\mathcal{U}_\xi(\mathfrak{sl}_2)/\ker \chi$ has dimension N^2 for any χ , and the whole center

$$Z(\mathcal{U}_\xi(\mathfrak{sl}_2)) = \mathcal{Z}_0[\Omega]/(\text{polynomial relation})$$

is generated by \mathcal{Z}_0 and the Casimir element Ω , modulo a degree N polynomial relation given by a Chebyshev polynomial. \diamond

Proof. See [McP21, Chapter 0] or [Bla+20, Section 6]. These results are due to work of De Concini, Kac, and Procesi [DKP91; DKP92]. \square

[DKP92] C. De Concini, V. G. Kac, and C. Procesi, “Quantum coadjoint action”. [DOI](#)

We can be more concrete by giving a presentation of $\mathcal{U}_q(\mathfrak{sl}_2)$: it is the algebra over $\mathbb{C}[q, q^{-1}]$ with generators $K^{\pm 1}, E, F$ and relations

$$KK^{-1} = 1, \quad KE = q^2 EK, \quad KF = q^{-2} FK, \quad EF - FE = (q - q^{-1})(K - K^{-1}).$$

It is a Hopf algebra with coproduct

$$\Delta(K) = K \otimes K, \quad \Delta(E) = E \otimes K + 1 \otimes E, \quad \Delta(F) = F \otimes 1 + K^{-1} \otimes F,$$

counit

$$\epsilon(K) = 1, \quad \epsilon(E) = \epsilon(F) = 0,$$

and antipode

$$S(E) = -EK^{-1}, \quad S(F) = -KF, \quad S(K) = K^{-1}.$$

For q not a root of unity, the center $Z(\mathcal{U}_q(\mathfrak{sl}_2))$ is generated by the *Casimir*

$$\Omega = EF + q^{-1}K + qK^{-1} = FE + qK + q^{-1}K^{-1}.$$

PROPOSITION 5.2. At $q = \xi$ a $2N$ th root of unity the subalgebra \mathcal{Z}_0 is generated by $K^{\pm N}, E^N$, and F^N . Characters $\chi : \mathcal{Z}_0 \rightarrow \mathbb{C}$ correspond to points of $\mathrm{SL}_2(\mathbb{C})^*$ via

$$\chi \mapsto \left(\begin{bmatrix} \chi(K^N) & 0 \\ \chi(K^N F^N) & 1 \end{bmatrix}, \begin{bmatrix} 1 & \chi(E^N) \\ 0 & \chi(K^N) \end{bmatrix} \right) \in \mathrm{SL}_2(\mathbb{C})^*$$

and this correspondence gives an isomorphism $\mathrm{Spec}(\mathcal{Z}_0) \rightarrow \mathrm{SL}_2(\mathbb{C})^*$ of algebraic groups. \diamond

As a consequence, to construct quantum invariants from $\mathcal{U}_\xi(\mathfrak{sl}_2)$ we must understand the group $\mathrm{SL}_2(\mathbb{C})^*$. To see why, use Schur’s Lemma: if V is any simple $\mathcal{U}_\xi(\mathfrak{sl}_2)$ -module, the action of the central subalgebra \mathcal{Z}_0 factors through some character $\chi : \mathcal{Z}_0 \rightarrow \mathbb{C}$. Furthermore, if V_1, V_2 are two simple modules with characters χ_1, χ_2 , then their tensor product $V_1 \otimes V_2$ will have central character $\chi_1 \chi_2$. One way to say this is that $\mathcal{U}_\xi(\mathfrak{sl}_2)\text{-Mod}$ is a $\mathrm{SL}_2(\mathbb{C})^*$ -*graded category*.¹⁶

¹⁶ Strictly speaking, this is the case for the category of finite-dimensional $\mathcal{U}_\xi(\mathfrak{sl}_2)$ -modules on which \mathcal{Z}_0 acts diagonalizably.

[RT91] N. Reshetikhin and V. G. Turaev, “Invariants of 3-manifolds via link polynomials and quantum groups”. [DOI](#)

[Tur16] V. G. Turaev, *Quantum invariants of knots and 3-manifolds*. [DOI](#)

One approach to dealing with this grading is to mostly eliminate it: if we take the quotient of $\mathcal{U}_\xi(\mathfrak{sl}_2)$ by the relations $K^{2N} = 1$, $E^N = F^N = 0$ we obtain the *small quantum group* $\overline{\mathcal{U}}_\xi$. This corresponds to considering only representations whose \mathcal{Z}_0 -character is plus or minus the identity element of $\mathrm{SL}_2(\mathbb{C})^*$. The category $\overline{\mathcal{U}}_\xi\text{-Mod}$ is not semisimple, but by killing the so-called negligible morphisms (those with quantum trace 0) we can obtain a *modular* category, which has the necessary algebraic properties to construct a surgery TQFT [RT91; Tur16]. The corresponding link invariants are colored Jones polynomials evaluated at roots of unity.

However, we want to go in a different direction and take full advantage of the $\mathrm{SL}_2(\mathbb{C})^*$ -grading. This idea leads to *quantum holonomy invariants* [KR05; Bla+20; McP22; McP21]. In the usual construction, picking a single $\mathcal{U}_\xi(\mathfrak{sl}_2)$ -module V gives a link invariant; for example, choosing V to be the simple N -dimensional representation of $\mathcal{U}_\xi(\mathfrak{sl}_2)$ gives the colored Jones polynomial at a root of unity [MM01]. For quantum holonomy invariants, we instead pick a *family*¹⁷ V_χ of $\mathcal{U}_\xi(\mathfrak{sl}_2)$ -modules indexed by points of $\mathrm{SL}_2(\mathbb{C})^*$. We think of V_χ as a deformation of V by the character $\chi \in \mathrm{SL}_2(\mathbb{C})^*$, and V is the case where χ is the identity element. The input to our construction is no longer a link diagram, but a link diagram with segments colored by elements of $\mathrm{SL}_2(\mathbb{C})^*$. As shown in Section 2, such a coloring is a choice of hyperbolic structure on the link complement, so we think of holonomy invariants as geometrically twisted versions of ordinary quantum invariants.

[McP22] C. McPhail-Snyder, “Holonomy invariants of links and nonabelian Reidemeister torsion”. [arXiv](#) [DOI](#)

¹⁷ This is what Blanchet et al. [Bla+20] call a *representation* of a biquandle in a pivotal category.

5.2. The braiding at a root of unity

In order for the construction described in the last paragraph to work the coloring by elements of $\mathrm{SL}_2(\mathbb{C})^*$ has to be compatible with the structure of $\mathcal{U}_\xi(\mathfrak{sl}_2)$, in particular with the braiding. For $q = \xi$ a root of unity there are some technical issues, which we briefly explain.

It is frequently said that $\mathcal{U}_q(\mathfrak{sl}_2)$ is a *quasitriangular* Hopf algebra, but strictly speaking this is false. Instead this is true for a version $\mathcal{U}_\hbar(\mathfrak{sl}_2)$ defined over formal power series in \hbar , where $q = e^\hbar$. Saying that the Hopf algebra $\mathcal{U}_\hbar(\mathfrak{sl}_2)$ is quasitriangular means in particular that it has a *universal R-matrix*

$$\mathbf{R} = q^{H \otimes H/2} \sum_{n=0}^{\infty} \frac{q^{n(n-1)/2}}{\{n\}!} (E \otimes F)^n \in \mathcal{U}_\hbar(\mathfrak{sl}_2) \otimes \mathcal{U}_\hbar(\mathfrak{sl}_2) \quad (25)$$

where $\{n\} := q^n - q^{-n}$ is a quantum integer and $\{n\}! := \{n\}\{n-1\} \cdots \{1\}$ is a quantum factorial. The key properties of \mathbf{R} are that it intertwines the coproduct and opposite coproduct

$$\mathbf{R}\Delta = \Delta^{\mathrm{op}}\mathbf{R}$$

and satisfies the *Yang-Baxter relation*

$$\mathbf{R}_{12}\mathbf{R}_{13}\mathbf{R}_{23} = \mathbf{R}_{23}\mathbf{R}_{13}\mathbf{R}_{12}$$

which is a version of the braid relation. (Here $\mathbf{R}_{12} = \mathbf{R} \otimes 1$ and so on.) Specifically, for any $\mathcal{U}_\hbar(\mathfrak{sl}_2)$ -module V , write R for the action of \mathbf{R} on $V \otimes V$, let $\tau(x \otimes y) = y \otimes x$. Then $c = \tau R$ is a map $V \otimes V \rightarrow V \otimes V$ of $\mathcal{U}_\hbar(\mathfrak{sl}_2)$ -modules satisfying the braid relation

$$(c \otimes \mathrm{id})(\mathrm{id} \otimes c)(c \otimes \mathrm{id}) = (\mathrm{id} \otimes c)(c \otimes \mathrm{id})(\mathrm{id} \otimes c).$$

The map c is the braiding used to define quantum link invariants.

Usually we work with $\mathcal{U}_q(\mathfrak{sl}_2)$, not $\mathcal{U}_\hbar(\mathfrak{sl}_2)$, even though the element \mathbf{R} involves power series in \hbar . It turns out that for any finite-dimensional $\mathcal{U}_q(\mathfrak{sl}_2)$ -module V the action of \mathbf{R}

converges and can be written in terms of q only, which gives the R -matrices defining the colored Jones polynomials. The reason this works is that when q is not a root of unity the elements E and F act nilpotently on any finite-dimensional representation.

Even when $q = \xi$ is a root of unity one can choose modules for which E and F act nilpotently. This leads to Kashaev's invariant [MM01] and to the ADO invariants [ADO92; Bla+16]. However, these modules correspond to $\mathrm{SL}_2(\mathbb{C})$ -structures with reducible or abelian image; to capture geometrically interesting $\mathrm{SL}_2(\mathbb{C})$ -structures we need to allow E and F to act invertibly, that is to consider *cyclic* $\mathcal{U}_\xi(\mathfrak{sl}_2)$ -modules. Unfortunately the action of the R -matrix (25) on a tensor product of two cyclic modules diverges. We can work around this by instead considering its conjugation action.

PROPOSITION 5.3. Consider the automorphism \mathcal{R} of $\mathcal{U}_h(\mathfrak{sl}_2)^{\otimes 2}$ given by

$$\mathcal{R}(x) := \mathbf{R}x\mathbf{R}^{-1}.$$

Write $W = 1 - K^{-N}E^N \otimes F^N K^N \in \mathcal{U}_\xi(\mathfrak{sl}_2)^{\otimes 2}$. Then \mathcal{R} defines an algebra homomorphism

$$\mathcal{R} : \mathcal{U}_\xi(\mathfrak{sl}_2)^{\otimes 2} \rightarrow \mathcal{U}_\xi(\mathfrak{sl}_2)^{\otimes 2}[W^{-1}]$$

characterized uniquely by

$$\begin{aligned}\mathcal{R}(1 \otimes K) &= (1 \otimes K)(1 - \xi^{-1}K^{-1}E \otimes FK) \\ \mathcal{R}(E \otimes 1) &= E \otimes K \\ \mathcal{R}(1 \otimes F) &= K^{-1} \otimes F\end{aligned}$$

and

$$\mathcal{R}(\Delta(u)) = \Delta^{\mathrm{op}}(u), \quad u \in \mathcal{U}_\xi(\mathfrak{sl}_2).$$

◇

The requirement that W be invertible is related to the fact that the shape biquandle is only partially defined.

Proof. See [KR04]. □

For a tensor product $V_1 \otimes V_2$ of $\mathcal{U}_\xi(\mathfrak{sl}_2)$ -modules the R -matrix defining the braiding is no longer given by the action of \mathbf{R} . Instead we say a linear map

$$R : V_1 \otimes V_2 \rightarrow V_{1'} \otimes V_{2'} \tag{26}$$

is a *holonomy R -matrix* if it intertwines \mathcal{R} in the sense that

$$R(x \cdot v) = \mathcal{R}(x) \cdot R(v) \text{ for every } v \in V_1 \otimes V_2, x \in \mathcal{U}_\xi(\mathfrak{sl}_2)^{\otimes 2}.$$

For irreducible V_1 and V_2 this characterizes R up to an overall scalar, but it is not obvious how to compute the matrix elements of R or to choose the normalization. This problem was the original motivation to consider the Weyl presentation of $\mathcal{U}_\xi(\mathfrak{sl}_2)$ discussed in the next section; a partial solution is given in the author's thesis [McP21, Chapter 3], and a full solution is forthcoming [MR22].

More relevant to us is the fact that the module $V_{1'} \otimes V_{2'}$ on the right-hand side of (26) will in general not be isomorphic to $V_1 \otimes V_2$. One way to see this is to consider their

[ADO92] Y. Akutsu, T. Deguchi, and T. Ohtsuki, "Invariants of colored links". [DOI](#)

[Bla+16] C. Blanchet et al., "Non-semi-simple TQFTs, Reidemeister torsion and Kashaev's invariants". [arXiv](#) [DOI](#)

[KR04] R. Kashaev and N. Reshetikhin, "Braiding for the quantum \mathfrak{gl}_2 at roots of unity". [arXiv](#) [DOI](#)

\mathcal{Z}_0 -characters: if V_1, V_2 have characters χ_1, χ_2 , then the action of any $z_1 \otimes z_2 \in \mathcal{Z}_0^{\otimes 2}$ will satisfy

$$\begin{aligned} (\chi_{1'} \otimes \chi_{2'})(z_1 \otimes z_2)R(v_1 \otimes v_2) &= z_1 \otimes z_2 \cdot R(v_1 \otimes v_2) \\ &= R(\mathcal{R}^{-1}(z_1 \otimes z_2)v_1 \otimes v_2) \\ &= (\chi_1 \otimes \chi_2)(\mathcal{R}^{-1}(z_1 \otimes z_2))R(v_1 \otimes v_2) \end{aligned}$$

so the characters $\chi_{1'}, \chi_{2'}$ of the image have

$$\chi_{1'} \otimes \chi_{2'} = (\chi_1 \otimes \chi_2)\mathcal{R}^{-1}.$$

In fact, using the defining relations of \mathcal{R} this uniquely defines $\chi_{1'}$ and $\chi_{2'}$, and the map

$$(\chi_1, \chi_2) \mapsto (\chi_{2'}, \chi_{1'})$$

is *exactly* the braiding defining the biquandle on $\mathrm{SL}_2(\mathbb{C})^*$ considered in [Bla+20, Section 6]. To obtain the shape biquandle, we need to use a specific presentation of $\mathcal{U}_\xi(\mathfrak{sl}_2)$.

5.3. Cluster algebras and the Weyl presentation

To better understand \mathcal{R} it helps to use a particular presentation of $\mathcal{U}_q(\mathfrak{sl}_2)$.

DEFINITION 5.4. The *extended Weyl algebra* is the algebra \mathcal{W}_q generated over $\mathbb{C}[q, q^{-1}]$ by a central invertible element z and invertible x, y subject to the relation

$$xy = q^2yx.$$

PROPOSITION 5.5. The map $\phi : \mathcal{W}_q \rightarrow \mathcal{U}_q(\mathfrak{sl}_2)$ given by

$$K \mapsto x \quad E \mapsto qy(z - x) \quad F \mapsto y^{-1}(1 - z^{-1}x^{-1})$$

is an algebra homomorphism. It acts on the Casimir by

$$\Omega \mapsto qz + (qz)^{-1}.$$

At a $2N$ th root of unity $q = \xi$ the center of \mathcal{W}_ξ is generated by x^N, y^N , and z . The automorphism ϕ takes the center of $\mathcal{U}_\xi(\mathfrak{sl}_2)$ to the center of \mathcal{W}_ξ . Explicitly,

$$\begin{aligned} \phi(K^N) &= x^N \\ \phi(E^N) &= y^N(x^N - z^N) \\ \phi(F^N) &= y^{-N}(1 - z^{-N}x^{-N}). \end{aligned} \quad \diamond$$

REMARK 5.6. This presentation was obtained from one given by Faddeev [Fad00] in terms of a quantum cluster algebra with generators w_1, w_2, w_3, w_4 . These generators q^2 -commute according to a certain quiver [SS19, Figure 4] associated to the triangulation of a punctured disc given in Figure 17a. It is known [Fad00; SS19] that this presentation explains the factorization of the R -matrix of $\mathcal{U}_q(\mathfrak{sl}_2)$ into four terms; a version of this works at a root of unity [McP21, Chapter 3], and we should think of this factorization as being associated to the four-term decomposition of the octahedron at a crossing of a link diagram. Kashaev's construction [Kas95] of link invariants from quantum dilogarithms is closely related.

[Fad00] L. Faddeev, “Modular double of a quantum group”. [arXiv](#)

[SS19] G. Schrader and A. Shapiro, “A cluster realization of $U_q(\mathfrak{sl}_n)$ from quantum character varieties”. [arXiv](#) [DOI](#)

¹⁸ Because z is central, not just z^N , a central character of \mathcal{W}_ξ at a $2N$ th root of unity specifies more than just a shape: there is an additional choice of an N th root of the meridian eigenvalue. The associated holonomy invariants depend on this choice, as discussed in Theorem 1.3.

The map ϕ sends central characters of \mathcal{W}_ξ to central characters of $\mathcal{U}_\xi(\mathfrak{sl}_2)$ via $\chi \mapsto \chi\phi$. If χ is a central character with $\chi(x^N) = a$, $\chi(y^N) = b$, and $\chi(z^N) = m$,¹⁸ the map ϕ identifies χ with

$$\left(\begin{bmatrix} a & 0 \\ (a - 1/m)/b & 1 \end{bmatrix}, \begin{bmatrix} 1 & (a - m)b \\ 0 & a \end{bmatrix} \right)$$

which is exactly the holonomy of the shape (a, b, m) associated to χ . We can similarly pull back the map \mathcal{R} along ϕ to give an automorphism \mathcal{R}^W of $\mathcal{W}_q^{\otimes 2}$ characterized by

$$\begin{aligned} \mathcal{R}^W(x_1) &= x_1 g, \\ \mathcal{R}^W(x_2) &= g^{-1} x_2, \\ \mathcal{R}^W(y_1^{-1}) &= y_2^{-1} + (y_1^{-1} - z_2^{-1} y_2^{-1}) x_2^{-1}, \\ \mathcal{R}^W(y_2) &= \frac{z_1}{z_2} y_1 + (y_2 - z_2^{-1} y_1) x_1, \\ \mathcal{R}^W(z_1) &= z_1 \\ \mathcal{R}^W(z_2) &= z_2 \end{aligned}$$

where

$$g = 1 - x_1^{-1} y_1 (z_1 - x_1) y_2^{-1} (x_2 - z_2^{-1}).$$

We can use \mathcal{R}^W to define a braiding on the central characters of \mathcal{W}_ξ , which will turn out to be exactly the braiding of Definition 2.4.

LEMMA 5.7. The action of \mathcal{R}^W on the center of $\mathcal{W}_\xi^{\otimes 2}$ is given by

$$\begin{aligned} \mathcal{R}^W(x_1^N) &= x_1^N G, \\ \mathcal{R}^W(x_2^N) &= x_2^N G^{-1}, \\ \mathcal{R}^W(y_1^{-N}) &= y_2^{-N} + \left(y_1^{-N} - \frac{y_2^{-N}}{z_2^N} \right) x_2^{-N}, \\ \mathcal{R}^W(y_2^N) &= \frac{z_1^N}{z_2^N} y_1^N + \left(y_2^N - \frac{y_1^N}{z_2^N} \right) x_1^N, \end{aligned}$$

where

$$G = 1 + x_1^{-N} \frac{y_1^N}{y_2^N} (x_1^N - z_1^N) (x_2^N - z_2^{-N})$$

with inverse action

$$\begin{aligned} (\mathcal{R}^W)^{-1}(x_1^N) &= x_1^N \tilde{G}^{-1}, \\ (\mathcal{R}^W)^{-1}(x_2^N) &= x_2^N \tilde{G}, \\ (\mathcal{R}^W)^{-1}(y_1^{-N}) &= \frac{z_1^N}{z_2^N} y_2^{-N} + (y_1^{-N} - z_1^N y_2^{-N}) x_2^N, \\ (\mathcal{R}^W)^{-1}(y_2^N) &= y_1^N + (y_2^N - z_1^N y_1^N) x_1^{-N}, \end{aligned}$$

where

$$\tilde{G} = 1 + x_2^{-N} \frac{y_1^N}{y_2^N} (x_1^N - z_1^N) (x_2^N - z_2^{-N}).$$

◇

THEOREM 5.8. Consider the map B^W defined on pairs of central characters of \mathcal{W}_ξ by

$$B^W(\chi_1, \chi_2) = (\chi_{1'}, \chi_{2'}), \text{ where } (\chi_{1'} \otimes \chi_{2'}) = (\chi_1 \otimes \chi_2) \mathcal{R}^{-1}.$$

Identifying central characters of \mathcal{W}_ξ with shapes via $\chi \mapsto (\chi(x^N), \chi(y^N), \chi(z^N))$, the map B^W is exactly the map B defined by (1-3). \diamond

Proof. We have

$$\begin{aligned} b_{1'}^{-1} &= \chi_{1'}(y^{-N}) \\ &= (\chi_1 \otimes \chi_2) \left(\frac{z_1^N}{z_2^N} y_2^{-N} + (y_1^{-N} - z_1^N y_2^{-N}) x_2^N \right) \\ &= \frac{m_1}{b_2 m_2} + \left(\frac{1}{b_1} - \frac{m_1}{b_2} \right) a_2 \end{aligned}$$

which after some algebraic manipulation gives the expression for $b_{1'}$ in (2). The other variables follow similarly. \square

REMARK 5.9. While it is possible to derive (4-6) by inverting the map B , it is much easier to compute them by repeating the above proof with \mathcal{R} .

6. GLUING EQUATIONS

The conditions (1-3) on the shapes at each crossing seem rather complicated. In practice, we can usually make some simplifications. For example, we have already seen that we only need to make one choice of m per link component. It is possible to go further and either eliminate the a -variables or the b -variables, as long as we avoid certain geometrically degenerate solutions. To make this precise, we introduce some terminology.

DEFINITION 6.1. Let L be a link in S^3 with c components. The *representation variety* of L is the set \mathfrak{R}_L of representations $\rho : \pi_1(S^3 \setminus L) \rightarrow \mathrm{SL}_2(\mathbb{C})$ of the link complement into $\mathrm{SL}_2(\mathbb{C})$.

Now suppose D is a diagram of L with s segments. We associate variables

$$a_1, \dots, a_s, b_1, \dots, b_s \in \mathbb{C} \setminus \{0\}$$

to the segments of D and variables

$$m_1, \dots, m_c \in \mathbb{C} \setminus \{0\}$$

to the components. Writing $C(i)$ for the component of segment i , we assign each segment the shape $\chi_i = (a_i, b_i, m_{C(i)})$. The *shape variety* of D is the set $\mathfrak{S}_L \subset (\mathbb{C} \setminus \{0\})^{2s+c}$ of shapings satisfying the relations of Definition 2.6.

In this language Theorem 2.17 says that there is an inclusion $\mathfrak{S}_D \hookrightarrow \mathfrak{R}_L$. The inclusion is not surjective, but it is effectively surjective: we usually only care about representations up to the conjugation action of $\mathrm{SL}_2(\mathbb{C})$, and Theorem 2.18 says that the $\mathrm{SL}_2(\mathbb{C})$ -orbit of every $\rho \in \mathfrak{R}_L$ intersects the image of \mathfrak{S}_D .

In this section we will define two smaller sets \mathfrak{A}_D and \mathfrak{B}_D and show that they map injectively into \mathfrak{S}_D . \mathfrak{B}_D comes from eliminating the a -variables in terms of the b -variables, but it only detects non-pinched solutions in the sense of Definition 2.8. To check membership in \mathfrak{B}_D we only need to check one equation in the b_i and m_i for each segment of D . In parallel, \mathfrak{A}_D comes from eliminating the b -variables in terms of the a -variables, and it only detects

non-degenerate solutions. The equations defining \mathfrak{A}_D are instead associated to the regions of the diagram D : for each region we check that a certain product involving a -variables and m -variables is 1. Because every pinched solution is degenerate, but not vice-versa, we have injective maps

$$\mathfrak{B}_D \hookrightarrow \mathfrak{A}_D \hookrightarrow \mathfrak{S}_D \hookrightarrow \mathfrak{R}_L$$

for any diagram D of L . There are examples of geometrically interesting points of \mathfrak{S}_D that do not lie in the image of \mathfrak{B}_D , but Theorem 3.10 says that every point of \mathfrak{S}_D with nontrivial (not ± 1) holonomy lies in the image of \mathfrak{A}_D .

6.1. The b -shape variety \mathfrak{B}_D and the segment equations

Let D be a diagram of L with c components and s segments. Associate variables b_1, \dots, b_s to the segments and m_1, \dots, m_c to the components of D ; as before this gives a tuple $(b_i, m_{C(i)})$ for each segment i of D . Now consider a crossing of D . If the crossing is not pinched (which can be checked in terms of the b_i and m_i alone), Lemma 2.10 determines the a -variables for each segment at the crossing.

DEFINITION 6.2. Because a segment is adjacent to two crossings, this procedure assigns two different a -variables to each segment. The *segment equation* of a segment says that the two a -variables agree. The *b -shape variety* \mathfrak{B}_D of the diagram D is the set of all $b_1, \dots, b_s, m_1, \dots, m_c$ satisfying the segment equations.

THEOREM 6.3. There is an inclusion $\mathfrak{B}_D \hookrightarrow \mathfrak{S}_D$ whose image consists of all non-pinched shapings of D . \diamond

Proof. The segment equations are written in terms of two of the three variables of the shapes $\chi_i = (a_i, b_i, m_i)$. When the segment equations are satisfied each segment is also assigned a well-defined a -variable, hence a shape. These assignments determine a shaping because the equations (7) imply the braiding relations $B(\chi_1, \chi_2) = (\chi_{2'}, \chi_{1'})$ at every positive crossing, and similarly for negative crossings.

We can only compute non-pinched shapings in this manner because at a pinched crossing the expressions appearing in (7) and (8) are indeterminate. Conversely, any non-pinched shaping determines a solution of the b -gluing equations by forgetting the a -variables. \square

EXAMPLE 6.4. Consider the diagram D of the figure-eight knot given in Figure 1. For simplicity, we restrict to the boundary-parabolic case where the meridian eigenvalue m is 1. We assign b -variables b_1, \dots, b_8 to the segments of D . The equation for segment 1 is

$$\frac{b_4}{b_5} \frac{b_1 - b_5}{b_1 - b_4} = \frac{b_5 - b_1}{b_6 - b_1}$$

Following [KKY18, Example 4.6] we see that there is a 3-parameter family of solutions given in terms of p, q, r by

$$(b_1, \dots, b_8) = \left(pr, pq(1 + q\Lambda), -\frac{pr\Lambda(1 + q\Lambda)}{1 - p}, \frac{pqr}{1 - p}, \right. \\ \left. -qr, r - qr, -\frac{pr(1 - q)\Lambda^2}{1 + p\Lambda}, \frac{pr}{1 + p\Lambda} \right)$$

where Λ satisfies $\Lambda^2 + \Lambda + 1$. The solution space is parametrized by one discrete parameter Λ and three continuous parameters p, q, r , which can be freely chosen as long as we avoid pinched crossings and all the b_i are nonzero.

Solving for all of \mathfrak{B}_D and not just the part with $m = 1$ is significantly more difficult. We discuss this further and compute more examples in Section 6.3.

REMARK 6.5. In general our solutions have three extra parameters. Kim, Kim, and Yoon [KKY18, Example 4.6] explain this as follows: one degree of freedom comes from the homogeneity of the segment equations in the b_i , while the other two come from the arbitrary locations of the extra ideal points P_{\pm} of the octahedral decomposition (Section 3).

6.2. The a -shape variety \mathfrak{A}_D and the region equations

Instead of using Lemma 2.10 to eliminate the a -variables, we can use Lemma 2.11 to eliminate the b -variables. However, it is most convenient to do this using a slightly different set of variables.

DEFINITION 6.6. Let D be a diagram of a link L with s segments; because D is a 4-valent planar graph there are $s - 1$ regions, one of which is unbounded. To any shaping of D we associate $s - 1$ *region variables* r_0, \dots, r_{s-2} by the rule given in Figure 30: when passing from r_i to $r_{i'}$ across a strand $\chi = (a, b, m)$ we should have $r_{i'} = ar_i$.

LEMMA 6.7. Any shaping of D gives well-defined region variables. \diamond

Proof. The rules of Definition 6.6 determine the r_i up to an overall constant from any shaping: we can walk from the unbounded region of D to any other region, picking up factors of a_i in the process. We need to make sure this assignment is well-defined.

It's enough to check it's well-defined near each crossing. Given a choice of r_N at a crossing (labeled as in Figure 3), we have both

$$r_S = a_1 a_2 r_N \text{ and } r_S = a_{1'} a_{2'} r_N.$$

However, these give the same value for r_S because by (1) and (4) we have $a_1 a_2 = a_{1'} a_{2'}$ at any crossing. \square

We want to work the other way and use the region variables (and meridian eigenvalues) to determine a shaping. Suppose D has c components and we have chosen meridian eigenvalues m_1, \dots, m_c and region variables r_0, \dots, r_{s-2} . Lemma 2.11 gives the ratios of the b -variables near any crossing; given an arbitrary choice of one b_i , this determines the rest of them, and should give a shaping. However, there is a consistency condition: for these ratios to come from an assignment of b -variables to each segment bounding a region, the product of the ratios (one from each corner) must be 1.

DEFINITION 6.8. Let D be a diagram with region variables $\{r_i\}$ and meridian eigenvalues $\{m_i\}$. At non-degenerate positive crossings, the *corner terms* are

$$\begin{aligned} f_N &= \frac{r_W r_E - r_N r_S}{(r_W - m_1 r_N)(r_E - r_N / m_2)} \\ f_W &= \frac{(r_N - r_W / m_1)(r_S - r_W / m_2)}{r_N r_S - r_W r_E} \\ f_S &= \frac{r_W r_E - r_N r_S}{(r_E - r_S / m_1)(r_W - m_2 r_S)} \\ f_E &= \frac{(r_S - m_1 r_E)(r_N - m_2 r_E)}{r_N r_S - r_W r_E} \end{aligned} \tag{27}$$

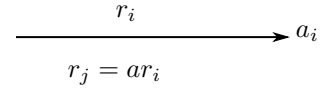


Figure 30: The correspondence between region variables and a -variables.

and at non-degenerate negative crossings they are

$$\begin{aligned}
 f_N &= \frac{(r_W - r_N/m_1)(r_E - m_2 r_N)}{r_W r_E - r_N r_S} \\
 f_W &= \frac{r_N r_S - r_W r_E}{(r_N - m_1 r_W)(r_S - m_2 r_W)} \\
 f_S &= \frac{(r_E - m_1 r_S)(r_W - r_S/m_2)}{r_W r_E - r_N r_S} \\
 f_E &= \frac{r_N r_S - r_W r_E}{(r_S - r_E/m_1)(r_N - r_E/m_2)}
 \end{aligned} \tag{28}$$

Here by r_N we mean the region variable north of the crossing (viewed left-to-right) as in Figure 3 and similarly for r_E, r_S, r_W . The *region equation* associated to any region of D says that the product of all the corner terms near a region is 1. We call the set \mathfrak{A}_D consisting of solutions $(r_0, \dots, r_{s-2}, m_1, \dots, m_2)$ to the region equations the *a-shape variety* of D . We require that solutions in D satisfy the non-degeneracy conditions, which in terms of the region variables are

$$r_W \neq m_1 r_N \tag{29}$$

EXAMPLE 6.9. In Figure 31 the central region labeled 7 has three segments and three corners. The corner terms are

$$\begin{aligned}
 f_{13} &= \frac{r_1 r_3 - r_2 r_7}{(r_3 - r_7/m_2)(r_1 - m_1 r_7)} \\
 f_{35} &= \frac{r_3 r_5 - r_4 r_7}{(r_5 - r_7/m_3)(r_3 - m_2 r_7)} \\
 f_{51} &= \frac{r_1 r_5 - r_6 r_7}{(r_1 - r_7/m_1)(r_5 - m_3 r_7)}
 \end{aligned}$$

and the region equation is

$$f_{13} f_{35} f_{51} = 1.$$

The non-degeneracy relations at each crossing are

$$r_1 r_3 \neq r_2 r_5, r_3 r_5 \neq r_4 r_7, \text{ and } r_1 r_5 \neq r_6 r_7.$$

REMARK 6.10. Because the region equations are homogeneous the region equations have an extra degree of freedom. We can remove this by fixing the variable for some region; an obvious choice is to fix the value for the unbounded region as $r_0 = 1$.

THEOREM 6.11. There is an inclusion $\mathfrak{A}_D \hookrightarrow \mathfrak{S}_D$ whose image consists of all non-degenerate shapings of D . \diamond

Proof. Lemma 6.7 says that any non-degenerate shaping determines a solution of the region equations. Conversely, a point of \mathfrak{A}_D is a choice of meridian eigenvalue m_i for each component and a choice of region variables, which uniquely determines the a -variables. The relations (9) and (10) determine the ratios between the b -variables of every segment, so if we pick the b -variable b_1 of one segment arbitrarily we determine all of them. \square

EXAMPLE 6.12. Consider the diagram of the trefoil knot in Figure 32 with labeled regions. For simplicity, assume that the meridian eigenvalue m is 1. Then the region equation for region 2 is

$$\frac{(r_4 - r_2)(r_1 - r_2)}{r_1 r_4 - r_0 r_2} \frac{(r_1 - r_2)(r_4 - r_2)}{r_1 r_4 - r_2 r_3} = 1$$

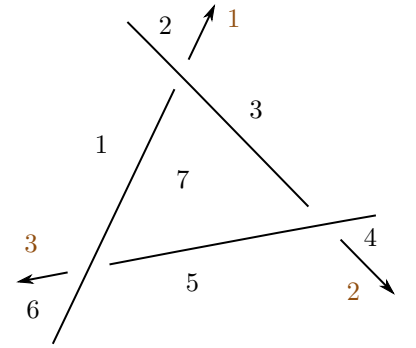


Figure 31: A diagram region with three edges.

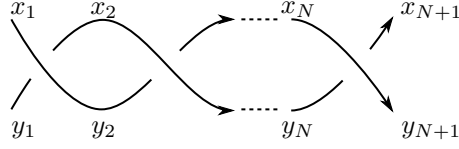


Figure 33: A parallel twist region with N positive crossings. Here we have labeled the b -variables of the top and bottom segments as x_i and y_i .

There are similar equations for the other regions. Two solutions to the region gluing equations are given by [KKY18, Example 4.11]

$$(r_0, r_1, r_2, r_3, r_4) = \left(1, \frac{(q-p)}{1+q-p}, \frac{q-p+pq}{1+q-p}, \frac{1+2q+pq}{1+q-p}, \frac{1+q+pq}{1+q-p} \right) \quad (30)$$

and

$$(r_0, r_1, r_2, r_3, r_4) = (1, p, 1, 1, 2-p) \quad (31)$$

Here we can choose p, q arbitrarily as long as the non-degeneracy conditions are satisfied. The first family of solutions has nonabelian holonomy, while the second is abelian. The abelian family does not correspond to a point of \mathfrak{B}_D because shapings with abelian holonomy are necessarily pinched.

6.3. The segment equations of a twist region

A *twist region* of a knot diagram with N positive twists is shown in Figure 33. We call it a *parallel* twist region because both strands are oriented in the same direction. Kim, Kim, and Yoon [KKY18, Section 6] showed how to solve the segment equations in a twist region in when the holonomy representation is boundary-parabolic (that is, when $m = \pm 1$). By doing so, they can compute boundary-parabolic $\mathrm{SL}_2(\mathbb{C})$ -structures on some infinite families of knots like $(2, N)$ torus knots and twist knots. In this section we translate their computation to our conventions and explain how to find all the $\mathrm{SL}_2(\mathbb{C})$ -structures on the $(2, N)$ torus knots, not just the boundary parabolic ones.

DEFINITION 6.13. A sequence $\{F_i\}_{i \in \mathbb{Z}}$ is *W -Fibonacci* for $W \in \mathbb{C}$ if it satisfies

$$F_{i+1} = W \cdot F_i + F_{i-1}.$$

The sequence $\{B_i\}$ with $B_0 = 0$ and $B_1 = 1$ is called the *base* W -Fibonacci sequence.

LEMMA 6.14. Let $\{F_i\}$ and $\{G_i\}$ be W -Fibonacci sequences and $\{B_i\}$ the base W -Fibonacci sequence. Then for all i ,

- (a) $F_i = F_0 B_{i-1} + F_1 B_i$,
- (b) $B_i^2 - B_{i-1} B_{i+1} = (-1)^{i+1}$,
- (c) and if $i \geq 0$

$$B_{i+1} = \sum_{0 \leq j \leq i/2} \binom{i-j}{j} W^{i-2j}. \quad \diamond$$

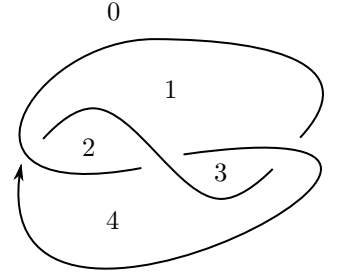


Figure 32: A diagram of the trefoil knot with labeled regions.

Proof. [KKY18, Lemma 6.2]. \square

LEMMA 6.15. Consider a parallel twist region with N positive twists, labeled as in Figure 33, in which both strands have meridian eigenvalue m . If the equations

$$x_i = \frac{F_i}{G_i} \quad y_i = \frac{F_{i-1}}{mG_{i+1}} \quad (32)$$

hold for $i = 1, 2$ (i.e. for segments 1, 2, 3, 4) then they hold for all $1 \leq i \leq n + 1$. In a region with n negative twists, the same holds with (32) replaced with

$$x_i = \frac{F_{i-1}}{G_{i+1}} \quad y_i = \frac{F_i}{mG_i} \quad \diamond \quad (33)$$

Proof. Consider the gluing equation for the segment labeled x_i . Because we are using b -variables, we think of the four b -variables associated to the segments at each crossing as determining the a -variables via (7). The gluing equation of a segment is then checking that the a -variables for each side agree. In this case, it is

$$\frac{x_{i-1}}{my_i} \frac{mx_i - y_i}{x_i - x_{i-1}} = \frac{y_i - mx_i}{x_{i+1} - x_i}$$

Solving for x_{i+1} and repeating this argument for the segment y_i gives the recurrence relations

$$\begin{aligned} x_{i+1} &= my_i - \frac{mx_i y_i}{x_{i-1}} + x_i \\ \frac{1}{y_{i+1}} &= \frac{m}{x_i} - \frac{my_{i-1}}{x_i y_i} + \frac{1}{y_i} \end{aligned}$$

(These are the relations of [KKY18, Lemma 6.3] up to some factors of m .) The result follows by induction, and the negative case works similarly.

To give some details, substitute (32) into the recurrence for x_{i+1} to obtain

$$\frac{F_{i+1}}{G_{i+1}} = \frac{F_{i-1}}{G_{i+1}} - \frac{F_i G_{i-1}}{G_i G_{i+1}} + \frac{F_i}{G_i}$$

equivalently

$$F_{i+1} = G_i^{-1} [G_i F_{i-1} + F_i (G_{i+1} - G_{i-1})]$$

After applying the recurrence for G_{i+1} the right-hand side becomes

$$\begin{aligned} G_i^{-1} [G_i F_{i-1} + F_i (WG_i + G_{i-1} - G_{i-1})] &= F_{i-1} + WF_i \\ &= F_{i+1} \end{aligned}$$

as required. Something similar works for the recurrence for y_i . \square

PROPOSITION 6.16. In a parallel twist region with positive twists in which both strands have meridian eigenvalue m , the adjusted segment variables are given in terms of x_1, x_2, y_1, y_2 by

$$x_i = \frac{mx_1 y_1 W \text{Fib}_{i-1}(W) + x_1 (x_2 - my_1) \text{Fib}_i(W)}{(x_2 - my_1) \text{Fib}_{i-2}(W) + x_1 W \text{Fib}_{i-1}(W)} \quad (34)$$

$$y_i = m^{-1} \frac{mx_1 y_1 W \text{Fib}_{i-2}(W) + x_1 (x_2 - my_1) \text{Fib}_{i-1}(W)}{(x_2 - my_1) \text{Fib}_{i-1}(W) + x_1 W \text{Fib}_i(W)} \quad (35)$$

where

$$W^2 = (my_1 - x_2) \left(\frac{1}{x_1} - \frac{1}{my_2} \right),$$

Fib_i is the polynomial $\text{Fib}_i(W) = B_i$, and B_i is the base W -Fibonacci sequence determined by

$$B_{i+1} = WB_i + B_{i-1}, B_1 = 1, B_0 = 0. \quad \diamond$$

REMARK 6.17. The Fib_i are sometimes called the *Fibonacci polynomials*. When i is odd $\text{Fib}_i(W)$ is a polynomial in W^2 , and when i is even $\text{Fib}_i(W)$ is W times a polynomial in W^2 . In particular, the solutions in (34–35) depend only on W^2 , not W .

Proof. We need to pick the right initial conditions for F_i and G_i . A convenient way to do this is to set

$$\begin{aligned} F_0 &= mWx_1y_1 & F_1 &= x_1(x_2 - my_1) \\ G_1 &= x_2 - my_1 & G_2 &= Wx_1. \end{aligned}$$

Then we can check that

$$x_i = \frac{F_i}{G_i} \text{ and } y_i = \frac{F_{i-1}}{mG_{i+1}}$$

holds for $i = 1, 2$, so by Lemma 6.15 they hold for all i . We can now apply (a) of Lemma 6.14 \square

REMARK 6.18. To compute more examples, we would need to extend this computation to:

1. parallel twist regions where the meridian eigenvalues m_1, m_2 on the two strands differ, and
2. to antiparallel twist regions in the boundary non-parabolic ($m \neq \pm 1$) case.

In fact, the segment equations in these two cases are closely related, because there is a simple formula [McP21, Definition 4.2] for reversing the orientation of a strand. Following [HL18, Section 7], the right generalization is to consider sequences of the form

$$A_{i+1} = WA_i + \frac{m_i}{m_{i+1}} A_{i-1}$$

where the index on m_i is understood mod 2.

We can at use Proposition 6.16 to compute an infinite family of boundary non-parabolic examples. A $(2, N)$ -torus knot is obtained by attaching segments x_1 and x_{N+1} and segments y_1 and y_{N+1} in Figure 33. We assume $N = 2n + 1$ is odd, so that we obtain a knot and not a link. We can now solve for its segment variables. We think of x_1, x_2 , and y_1 as parameters and use the ansatz

$$x_i = \frac{F_i}{G_i} \text{ and } y_i = \frac{F_{i-1}}{mG_{i+1}}$$

of Proposition 6.16. We need to choose Λ (equivalently, choose y_2) so that the gluing equations of the edges $x_1 = x_{N+1}$ and $y_1 = y_{N+1}$ are satisfied. The former is

$$\frac{x_N}{my_1} \frac{mx_1 - y_1}{x_1 - x_N} = \frac{y_1 - mx_1}{x_2 - x_1}$$

or

$$1 = \frac{x_N}{my_1} \frac{x_1 - x_2}{x_1 - x_N}$$

[HL18] J.-Y. Ham and J. Lee, *On the volume and the Chern-Simons invariant for the hyperbolic alternating knot orbifolds*. [arXiv](#)

which is equivalent to

$$\frac{G_N}{F_N} = \frac{G_0}{F_0}. \quad (36)$$

Now, the sequence $H_i = F_0 G_i - F_i G_0$ is a $\sqrt{\Lambda}$ -Fibonacci sequence satisfying $H_0 = 0$ and $H_1 \neq 0$, and (36) holds if and only if $H_N = 0$. By part (a) of Lemma 6.14 we have $H_i = H_1 B_i$ for all i , and we conclude that (36) holds if and only if $B_N = 0$. Using the fact that $N = 2n + 1$ is odd, the condition is

$$\begin{aligned} B_{2n+1} &= \sum_{0 \leq j \leq (2n+1)/2} \binom{2n-j}{j} \sqrt{\Lambda}^{2n-2j} \\ &= \sum_{0 \leq j \leq n} \binom{2n-j}{j} \Lambda^{n-j} \end{aligned}$$

It turns out that this also implies the gluing relation for $y_1 = y_{N+1}$. We have shown:

THEOREM 6.19. Taking the braid closure of Figure 33 for $N = 2n + 1$ gives a diagram D of a $(2, 2n + 1)$ -torus knot. For any meridian eigenvalue m the b -variables of a shaping of D are given by

$$x_i = \frac{q\sqrt{\Lambda} \text{Fib}_{i-1}(\sqrt{\Lambda}) + pr \text{Fib}_i(\sqrt{\Lambda})}{r \text{Fib}_{i-2}(\sqrt{\Lambda}) + \sqrt{\Lambda} \text{Fib}_{i-1}(\sqrt{\Lambda})} \quad (37)$$

$$y_i = \frac{1}{m} \frac{q\sqrt{\Lambda} \text{Fib}_{i-2}(\sqrt{\Lambda}) + pr \text{Fib}_{i-1}(\sqrt{\Lambda})}{r \text{Fib}_{i-1}(\sqrt{\Lambda}) + \sqrt{\Lambda} \text{Fib}_i(\sqrt{\Lambda})} \quad (38)$$

where Λ satisfies

$$\sum_{0 \leq j \leq n} \binom{2n-j}{j} \Lambda^{n-j} = 0 \quad (39)$$

and

$$p = x_1, \quad q = my_1, \quad r = (x_2 - my_1)/x_1$$

are arbitrary nonzero parameters chosen so that the first crossing is not pinched.¹⁹ As discussed in Remark 6.17 the expressions for x_i and y_i depend only on Λ , not $\sqrt{\Lambda}$. \diamond

REMARK 6.20. The polynomial in (39) is sometimes called the *Riley polynomial* of the knot, and this specific case is discussed in [Ril72, Section 5]. In particular, (39) is a monic polynomial with n distinct roots, which corresponds to the general fact [Muñ09, Theorem 3.1] that the character variety of a (p, q) torus knot has $(p-1)(q-1)/2$ components coming from irreducible representations.²⁰ In our family of examples $p = 2$ and $q = 2n + 1$.

The roots of (39) can be given explicitly [Ril72, Theorem 5]. In particular, when $n = 1$ the only root is $\Lambda = -1$. This gives us the solutions (40) for the trefoil knot.

REMARK 6.21. The geometry of these solutions is not affected by the choice of p, q, r , but is instead determined by m and the choice of root Λ of the Riley polynomial. In our conventions this is less obvious, but there is a different presentation [KKY18, Section 5] of the holonomy of a shaped diagram that is manifestly independent of the choice of p, q, r .

We can still give an informal explanation of this independence. The components of the character variety of a torus knot corresponding to irreducible holonomy representations are all 1-dimensional [Muñ09, Theorem 3.1]. Picking the discrete parameter Λ determines the component, which is then parametrized by a rational function of m . (The components are isomorphic to \mathbb{C} via the trace $\mu + \mu^{-1}$ of a generator of the knot group, but this generator is not a meridian, so μ is some rational function of m .)

¹⁹ p, q, r are closely related to but not exactly the variables p, q, r in [KKY18, Theorem 6.5].

[Ril72] R. Riley, “Parabolic representations of knot groups. I”. [DOI](#)

[Muñ09] V. Muñoz, “The $\text{SL}(2, \mathbb{C})$ -character varieties of torus knots”. [arXiv](#) [DOI](#)

²⁰ There is also a component describing the representations with abelian image. It is not detected by the b -gluing equations because they only detect non-pinched solutions, which always correspond to a nonabelian holonomy representation.

EXAMPLE 6.22. Consider the diagram of the trefoil in Figure 4. For any meridian eigenvalue $m \neq 0$, we can freely choose the variables b_1, b_2, b_3 , as long as

$$\frac{b_2}{mb_1}, \frac{b_3}{b_1} \neq 1$$

so that the solution is not pinched. The remaining segment variables are given by

$$(b_4, b_5, b_6) = \left(\frac{b_1(mb_2 - b_3)}{m(b_1 + mb_2 - b_3)}, \frac{mb_1b_2}{b_1 + mb_2 - b_3}, -\frac{b_1b_3}{m(mb_2 - b_3)} \right). \quad (40)$$

This solution is the case $n = 1$ of Theorem 6.19 after the substitutions $p = b_1, q = mb_2, r = (b_3 - mb_2)/b_1$.

We can use Theorem 4.4 to compute the boundary eigenvalues of this representation. We have $\delta(\mathfrak{m}) = m$ and

$$\ell = \delta(\mathfrak{l}) = m^{-3} \frac{b_2b_4b_6}{b_1b_3b_5} = -1/m^6$$

which matches the A -polynomial $m^6\ell + 1$ of the trefoil knot.

As before, the choice of b_1, b_2, b_3 does not affect the conjugacy class of the $\mathrm{SL}_2(\mathbb{C})$ -structure, which is uniquely determined by m . In this case, we can check this against the character variety of the trefoil knot. Non-pinched solutions correspond to $\mathrm{SL}_2(\mathbb{C})$ -structures with nonabelian image, and the $\mathrm{SL}_2(\mathbb{C})$ -character variety of the trefoil has a single nonabelian component [Muñ09, Theorem 3.1] cut out by the equation

$$m^6\ell + 1 = 0.$$

This shows explicitly that (40) yields at least one $\mathrm{SL}_2(\mathbb{C})$ -structure in every nonabelian conjugacy class. We can do a similar computation for general $(2, 2n + 1)$ -torus knots:

EXAMPLE 6.23. Consider the shaping of the $(2, N)$ -torus knot given in Theorem 6.19. The longitude is

$$\begin{aligned} \delta(\mathfrak{l}) &= \frac{1}{m^N} \prod_{k=1}^N \frac{x_i}{y_i} = \frac{1}{m^N} \prod_{k=1}^N \frac{F_{k-1}}{mG_{k+1}} \frac{G_k}{F_k} \\ &= \frac{1}{m^{2N}} \frac{F_0G_1}{F_NG_{N+1}} = \frac{1}{m^{2N}} \frac{G_0G_1}{G_NG_{N+1}}, \end{aligned}$$

where in the last step we used (36). Because $B_N = 0$, by Lemma 6.14 we have

$$\begin{aligned} \frac{G_0G_1}{G_NG_{N+1}} &= \frac{G_0G_1}{(G_0B_{N-1} + G_1B_N)(G_0B_N + G_1B_{N+1})} \\ &= \frac{1}{B_{N-1}B_N} = (-1)^N = -1 \end{aligned}$$

because $N = 2n + 1$ is odd. We conclude that

$$\delta(\mathfrak{l}) = -m^{-2N} \quad (41)$$

which recovers the A -polynomial of the right-handed $(2, N)$ -torus knot.

The discrete parameter Λ does not appear in this computation; this corresponds to the fact [Muñ09, Theorem 3.1] that the n nonabelian components of the character variety are all isomorphic. Choosing Λ picks out a component which is then continuously parametrized by $m + m^{-1}$.

REFERENCES

- [ADO92] Yasuhiro Akutsu, Tetsuo Deguchi, and Tomotada Ohtsuki. “Invariants of colored links”. English. In: *Journal of Knot Theory and its Ramifications* 1.2 (1992), pp. 161–184. ISSN: 0218-2165. DOI: [10.1142/S0218216592000094](https://doi.org/10.1142/S0218216592000094).
- [Bla+16] Christian Blanchet, Francesco Costantino, Nathan Geer, and Bertrand Patureau-Mirand. “Non-semi-simple TQFTs, Reidemeister torsion and Kashaev’s invariants”. English. In: *Advances in Mathematics* 301 (2016), pp. 1–78. ISSN: 0001-8708. DOI: [10.1016/j.aim.2016.06.003](https://doi.org/10.1016/j.aim.2016.06.003). arXiv: [1404.7289](https://arxiv.org/abs/1404.7289) [math.GT].
- [Bla+20] Christian Blanchet, Nathan Geer, Bertrand Patureau-Mirand, and Nicolai Reshetikhin. “Holonomy braidings, biquandles and quantum invariants of links with $SL_2(\mathbb{C})$ flat connections”. In: *Selecta Mathematica* 26.2 (Mar. 2020). DOI: [10.1007/s00029-020-0545-0](https://doi.org/10.1007/s00029-020-0545-0). arXiv: [1806.02787v1](https://arxiv.org/abs/1806.02787v1) [math.GT].
- [Cal06] Danny Calegari. “Real places and torus bundles”. English. In: *Geometriae Dedicata* 118 (2006), pp. 209–227. ISSN: 0046-5755. DOI: [10.1007/s10711-005-9037-9](https://doi.org/10.1007/s10711-005-9037-9). arXiv: [math/0510416](https://arxiv.org/abs/math/0510416) [math.GT].
- [Cho16] Jinseok Cho. “Optimistic limit of the colored Jones polynomial and the existence of a solution”. English. In: *Proceedings of the American Mathematical Society* 144.4 (2016), pp. 1803–1814. ISSN: 0002-9939. DOI: [10.1090/proc/12845](https://doi.org/10.1090/proc/12845). arXiv: [1410.0525](https://arxiv.org/abs/1410.0525) [math.GT].
- [Cho18] Jinseok Cho. “Quandle theory and the optimistic limits of the representations of link groups”. In: *Pacific J. Math.* 295.2 (2018), pp. 329–366. ISSN: 0030-8730. DOI: [10.2140/pjm.2018.295.329](https://doi.org/10.2140/pjm.2018.295.329). arXiv: [1409.1764](https://arxiv.org/abs/1409.1764) [math.GT].
- [CS83] Marc Culler and Peter B. Shalen. “Varieties of group representations and splittings of 3-manifolds”. English. In: *Annals of Mathematics. Second Series* 117 (1983), pp. 109–146. ISSN: 0003-486X. DOI: [10.2307/2006973](https://doi.org/10.2307/2006973).
- [Cul+] Marc Culler, Nathan M. Dunfield, Matthias Goerner, and Jeffrey R. Weeks. *SnapPy, a computer program for studying the geometry and topology of 3-manifolds*. Available at <http://snappy.computop.org>.
- [CYZ20] Jinseok Cho, Seokbeom Yoon, and Christian K. Zickert. “On the Hikami-Inoue conjecture”. English. In: *Algebraic & Geometric Topology* 20.1 (2020), pp. 279–301. ISSN: 1472-2747. DOI: [10.2140/agt.2020.20.279](https://doi.org/10.2140/agt.2020.20.279). arXiv: [1805.11841](https://arxiv.org/abs/1805.11841) [math.GT].
- [DKP91] Corrado De Concini, Victor G Kac, and C Procesi. “Representations of quantum groups at roots of 1”. In: *Modern quantum field theory (Bombay, 1990)* (1991), pp. 333–335.
- [DKP92] C. De Concini, V. G. Kac, and C. Procesi. “Quantum coadjoint action”. In: *Journal of the American Mathematical Society* 5.1 (1992), pp. 151–189. ISSN: 0894-0347. DOI: [10.2307/2152754](https://doi.org/10.2307/2152754).
- [Fad00] Ludwig Faddeev. “Modular double of a quantum group”. English. In: *Conférence Moshé Flato 1999: Quantization, deformation, and symmetries, Dijon, France, September 5–8, 1999. Volume I*. Dordrecht: Kluwer Academic Publishers, 2000, pp. 149–156. ISBN: 0-7923-6540-2. arXiv: [math/9912078](https://arxiv.org/abs/math/9912078) [math.QA].

- [GTZ15] Stavros Garoufalidis, Dylan P. Thurston, and Christian K. Zickert. “The complex volume of $SL(n, \mathbb{C})$ -representations of 3-manifolds”. English. In: *Duke Mathematical Journal* 164.11 (2015), pp. 2099–2160. ISSN: 0012-7094. DOI: [10.1215/00127094-3121185](https://doi.org/10.1215/00127094-3121185). arXiv: [1111.2828](https://arxiv.org/abs/1111.2828) [math.GT].
- [HI15] Kazuhiro Hikami and Rei Inoue. “Braids, complex volume and cluster algebras”. English. In: *Algebraic & Geometric Topology* 15.4 (2015), pp. 2175–2194. ISSN: 1472-2747. DOI: [10.2140/agt.2015.15.2175](https://doi.org/10.2140/agt.2015.15.2175). arXiv: [1304.4776](https://arxiv.org/abs/1304.4776) [math.GT].
- [HL18] Ji-Young Ham and Joongul Lee. *On the volume and the Chern-Simons invariant for the hyperbolic alternating knot orbifolds*. Mar. 3, 2018. arXiv: [1803.01259](https://arxiv.org/abs/1803.01259) [math.GT].
- [Kas95] Rinat Kashaev. “A link invariant from quantum dilogarithm”. In: *Modern Physics Letters A* 10.19 (June 1995), pp. 1409–1418. DOI: [10.1142/s0217732395001526](https://doi.org/10.1142/s0217732395001526). arXiv: [q-alg/9504020](https://arxiv.org/abs/q-alg/9504020) [math.QA].
- [KKY18] Hyuk Kim, Seonhwa Kim, and Seokbeom Yoon. “Octahedral developing of knot complement. I: Pseudo-hyperbolic structure”. English. In: *Geometriae Dedicata* 197 (2018), pp. 123–172. ISSN: 0046-5755. DOI: [10.1007/s10711-018-0323-8](https://doi.org/10.1007/s10711-018-0323-8). arXiv: [1612.02928v3](https://arxiv.org/abs/1612.02928v3) [math.GT].
- [KKY19] Hyuk Kim, Seonhwa Kim, and Seokbeom Yoon. *Octahedral developing of knot complement II: Ptolemy coordinates and applications*. Apr. 14, 2019. arXiv: [1904.06622](https://arxiv.org/abs/1904.06622) [math.GT].
- [KR04] R. Kashaev and N. Reshetikhin. “Braiding for the quantum gl_2 at roots of unity”. In: *Noncommutative Geometry and Representation Theory in Mathematical Physics*. Oct. 6, 2004. DOI: <http://dx.doi.org/10.1090/conm/391>. arXiv: [math/0410182v1](https://arxiv.org/abs/math/0410182v1) [math.QA].
- [KR05] R. Kashaev and N. Reshetikhin. “Invariants of tangles with flat connections in their complements”. In: *Graphs and Patterns in Mathematics and Theoretical Physics*. American Mathematical Society, 2005, pp. 151–172. DOI: [10.1090/pspum/073/2131015](https://doi.org/10.1090/pspum/073/2131015). arXiv: [1008.1384](https://arxiv.org/abs/1008.1384) [math.QA].
- [McP21] Calvin McPhail-Snyder. “ $SL_2(\mathbb{C})$ -holonomy invariants of links”. PhD thesis. UC Berkeley, May 2021. arXiv: [2105.05030](https://arxiv.org/abs/2105.05030) [math.QA].
- [McP22] Calvin McPhail-Snyder. “Holonomy invariants of links and nonabelian Reidemeister torsion”. In: *Quantum Topology* 13.1 (Mar. 2022), pp. 55–135. DOI: [10.4171/qt/160](https://doi.org/10.4171/qt/160). arXiv: [2005.01133v1](https://arxiv.org/abs/2005.01133v1) [math.QA].
- [MM01] Hitoshi Murakami and Jun Murakami. “The colored Jones polynomials and the simplicial volume of a knot”. In: *Acta Mathematica* 186.1 (2001), pp. 85–104. DOI: [10.1007/bf02392716](https://doi.org/10.1007/bf02392716). arXiv: [math/9905075](https://arxiv.org/abs/math/9905075) [math.GT].
- [MR22] Calvin McPhail-Snyder and Nicolai Reshetikhin. “The R -matrix for cyclic quantum sl_2 -modules”. 2022. In preparation.
- [Muñ09] Vicente Muñoz. “The $SL(2, \mathbb{C})$ -character varieties of torus knots”. In: *Rev. Mat. Complut.* 22.2 (2009), pp. 489–497. ISSN: 1139-1138. DOI: [10.5209/rev_REMA.2009.v22.n2.16290](https://doi.org/10.5209/rev_REMA.2009.v22.n2.16290). arXiv: [0901.1783](https://arxiv.org/abs/0901.1783) [math.AG].
- [Oht01] Tomotada Ohtsuki. *Quantum Invariants*. World Scientific, Nov. 2001. DOI: [10.1142/4746](https://doi.org/10.1142/4746).
- [Pur20] Jessica S. Purcell. *Hyperbolic knot theory*. English. Vol. 209. Providence, RI: American Mathematical Society (AMS), 2020, pp. xviii + 369. ISBN: 978-1-4704-5499-9; 978-1-4704-6211-6. DOI: [10.1090/gsm/209](https://doi.org/10.1090/gsm/209). arXiv: [2002.12652](https://arxiv.org/abs/2002.12652) [math.GT].

- [Ril72] Robert Riley. “Parabolic representations of knot groups. I”. English. In: *Proceedings of the London Mathematical Society. Third Series* 24 (1972), pp. 217–242. ISSN: 0024-6115. DOI: [10.1112/plms/s3-24.2.217](https://doi.org/10.1112/plms/s3-24.2.217).
- [RT90] N. Yu. Reshetikhin and V. G. Turaev. “Ribbon graphs and their invariants derived from quantum groups”. English. In: *Communications in Mathematical Physics* 127.1 (1990), pp. 1–26. ISSN: 0010-3616. DOI: [10.1007/BF02096491](https://doi.org/10.1007/BF02096491).
- [RT91] N. Reshetikhin and V. G. Turaev. “Invariants of 3-manifolds via link polynomials and quantum groups”. English. In: *Inventiones Mathematicae* 103.3 (1991), pp. 547–597. ISSN: 0020-9910. DOI: [10.1007/BF01239527](https://doi.org/10.1007/BF01239527).
- [SS19] Gus Schrader and Alexander Shapiro. “A cluster realization of $U_q(\mathfrak{sl}_n)$ from quantum character varieties”. English. In: *Inventiones Mathematicae* 216.3 (2019), pp. 799–846. ISSN: 0020-9910. DOI: [10.1007/s00222-019-00857-6](https://doi.org/10.1007/s00222-019-00857-6). arXiv: [1607.00271](https://arxiv.org/abs/1607.00271) [math.QA].
- [Thu02] William Thurston. *The geometry and topology of three-manifolds*. Electronic. Mar. 2002. URL: <http://library.msri.org/books/gt3m/>.
- [Thu99] Dylan Thurston. *Hyperbolic volume and the Jones polynomial*. 1999. URL: <https://dpthurst.pages.iu.edu/speaking/Grenoble.pdf>. Unpublished lecture notes.
- [Tur16] Vladimir G. Turaev. *Quantum invariants of knots and 3-manifolds*. English. Vol. 18. De Gruyter Studies in Mathematics. Berlin: Walter de Gruyter, 2016, pp. xii + 596. ISBN: 9783110435221. DOI: [10.1515/9783110435221](https://doi.org/10.1515/9783110435221).
- [Yoo18] Seokbeom Yoon. *The volume and Chern-Simons invariant of a Dehn-filled manifold*. Jan. 25, 2018. DOI: [10.1016/j.topol.2019.02.004](https://doi.org/10.1016/j.topol.2019.02.004). arXiv: [1801.08288](https://arxiv.org/abs/1801.08288) [math.GT].
- [Yoo21] Seokbeom Yoon. “On the potential functions for a link diagram”. English. In: *Journal of Knot Theory and its Ramifications* 30.7 (2021). Id/No 2150056, p. 24. ISSN: 0218-2165. DOI: [10.1142/S0218216521500565](https://doi.org/10.1142/S0218216521500565). arXiv: [1810.09080](https://arxiv.org/abs/1810.09080) [math.GT].